1994-06

Simulations of the high average power selene free electron laser prototype

Quick, Dennis D.

Monterey, California. Naval Postgraduate School

Approved for public release: distribution is unlimited.

SIMULATIONS OF THE HIGH AVERAGE POWER SELENE FREE ELECTRON LASER PROTOTYPE

by

Dennis D. Quick

Lieutenant, United States Navy

B. S., Illinois Institute of Technology, 1986

Submitted in partial fulfillment of the

requirements for the degree of

MASTER OF SCIENCE IN APPLIED PHYSICS

from the

NAVAL POSTGRADUATE SCHOOL

June 1994

REPORT DOCUMENTATION PAGE

1a. REPORT SECURITY CLASSIFICATION Unclassifed		1b. RESTRICTIVE MARKINGS	
2a. SECURITY CLASSIFICATION AUTHORITY		3. DISTRIBUTION/ AVAILABILITY OF REPORT Approved for public release; distribution is unlimited.	
2b. DECLASSIFICATION/DOWNGRADING SCHEDULE			
4. PERFORMING ORGANIZATION REPORT NUMBER(S)		5. MONITORING ORGANIZATION REPORT NUMBER(S)	
6a. NAME OF PERFORMING ORGANIZATION Naval Postgraduate School	6b. OFFICE SYMBOL *(If Applicable)* 33	7a. NAME OF MONITORING ORGANIZATION	
6c. ADDRESS *(city, state, and ZIP code)* Monterey, CA 93943-5000		7b. ADDRESS *(city, state, and ZIP code)*	
8a. NAME OF FUNDING/SPONSORING ORGANIZATION Naval Postgraduate School	6b. OFFICE SYMBOL *(If Applicable)* PH/Co	9. PROCUREMENT INSTRUMENT IDENTIFICATION NUMBER	
8c. ADDRESS *(city, state, and ZIP code)* Monterey, CA 93943-5000		10. SOURCE OF FUNDING NUMBERS	
		PROGRAM ELEMENT NO.	PROJECT NO.
			TASK NO.
			WORK UNIT ACCESSION NO.

11. TITLE *(Include Security Classification)* SIMULATIONS OF THE HIGH AVERAGE POWER SELENE FREE ELECTRON LASER PROTOTYPE(UNCLASSIFIED)

12. PERSONAL AUTHOR(S)
Quick, Dennis D.

13a. TYPE OF REPORT Master's Thesis	13b. TIME COVERED FROM TO	14. DATE OF REP*(year, month,day)* June, 1994	15. PAGE COUNT 63

16. SUPPLEMENTARY NOTATION
The views expressed in this thesis are those of the author and do not reflect the official policy or position of the Department of Defense or the U.S. Government.

17. COSATI CODES			18. SUBJECT TERMS *(continue on reverse if necessary and identify by block number)*
FIELD	GROUP	SUBGROUP	FEL,free electron laser,SELENE,optical klystron,directed energy,power beaming

19. ABSTRACT *(Continue on reverse if necessary and identify by block number)*

Free electron laser (FEL) technology continues to advance, providing alternative solutions to existing and potential problems. The capabilities of an FEL with respect to tunability, power and efficiency make it an attractive choice when moving into new laser utilization fields. The initial design parameters, for any new system, offer a good base to begin system simulation tests in an effort to determine the best possible design.

This is a study of the Novosibirsk design which is a prototype for the proposed SELENE FEL. The design uses a three-section, low-power optical klystron followed by a single-pass, high-power radiator. This system is inherently sensitive to electron beam quality, but affords flexibility in achieving the final design. The performance of the system is studied using the initial parameters.

An FEL, configured as a simple, two section optical klystron is studied to determine the basic operating characteristics of a high current FEL klystron

20. DISTRIBUTION/AVAILABILITY OF ABSTRACT [X] UNCLASSIFIED/UNLIMITED [ ] SAME AS RPT. [ ] DTIC USERS	21. ABSTRACT SECURITY CLASSIFICATION Unclassified	
22a. NAME OF RESPONSIBLE INDIVIDUAL W. B. Colson	22b. TELEPHONE (Include Area Code) (408) 656-2896	22c. OFFICE SYMBOL Code PH/Co

DD FORM 1473, 84 MAR 83 APR edition may be used until exhausted SECURITY CLASSIFICATION OF THIS PAGE
All other editions are obsolete Unclassified

ABSTRACT

Free electron laser (FEL) technology continues to advance, providing alternative solutions to existing and potential problems. The capabilities of an FEL with respect to tunability, power and efficiency make it an attractive choice when moving into new laser utilization fields. The initial design parameters, for any new system, offer a good base to begin system simulation tests in an effort to determine the best possible design.

This is a study of the Novosibirsk design which is a prototype for the proposed SELENE FEL. The design uses a three-section, low-power optical klystron followed by a single-pass, high-power radiator. This system is inherently sensitive to electron beam quality, but affords flexibility in achieving the final design. The performance of the system is studied using the initial parameters.

An FEL, configured as a simple, two section optical klystron is studied to determine the basic operating characteristics of a high current FEL klystron.

Table of Contents

ACKNOWLEDGEMENT

The author is thankful for support of this work by the Naval Postgraduate School. The author would like to express his gratitude to W. B. Colson for his invaluable instruction and guidance, R. L. Armstead for his thesis prep assistance and Mr. and Mrs. H. E. Bennett for their kindness and moral support.

I. INTRODUCTION

The military of today faces an increasingly difficult challenge in trying to defend against state-of-the-art weapons. These new threats travel with large velocities and pin-point accuracy requiring a defensive system that can not only detect and classify the threat, but track and engage during a very limited time window. Current gun and missile technology has progressed to near the limits of capability. The cost of enhanced performance has become extremely high, while the gains in performance are slight. The best approach for new weapons design is to pursue a system with "light speed" capability. This leads to a re-evaluation of laser technology.

Current shipboard anti-air defense is characterized as "layered defense." An incoming target is detected and engaged as far away as possible. The initial engagement weapon is the long and/or medium range missile followed by the 5"/54 or the 76 mm OTO Melara naval guns, depending on how the ship is equipped. Short range anti-missile missiles such as RAM and SEA SPARROW provide another layer of protection. RAM is not yet available and SEA SPARROW is being replaced by CIWS. The final weapon is the Vulcan/Phalanx Close In Weapons System (CIWS) which is a closed-loop fire control system directing a 6 barrel, 20 mm gatling gun. This system is designed to engage targets which are a threat to the ship and have leaked through the outer defenses. The availability of missiles and guns varies from ship to ship, however CIWS is present on nearly all naval vessels. On some, CIWS provides the only anti-air capability at hand.

A variety of threats must be dealt with. Long and short range surface-to-surface and air-to-surface missiles traveling at speeds from subsonic to Mach 3 or greater, and at altitudes from "sea skimming" to 20 km provide the need for

flexibility. Additionally, low, slow flying aircraft allow for terrorist type attacks. The low, slow flyers and the sea skimmer missiles can get fairly close before detection. This may be inside of the minimum range required for engagement with our own missiles. The naval gun systems are more suited for shore bombardment and anti-ship missions than anti-air. Short range missile systems are not prevalent throughout the fleet, leaving only CIWS.

CIWS has a reliable detection range of about 5000 m and an effective engagement range of about 2000 m. A typical missile requires a number of hits from CIWS before it is destroyed. This allows it to close to within 600 m before it comes apart. Even if the warhead is defeated, shrapnel damage from the flying pieces can be significant. An additional problem arises if the incoming missile can maneuver or "jink" around, throwing off the aim. This problem can prove almost insurmountable regardless of the defensive system in use. The finite flight time of the interceptor allows the target to make unanticipated alterations in its course resulting in a miss. Now, two problems are defined; lack of an engagement weapon for the period when the target is inside of medium weapons range but outside of CIWS engagement range, and unanticipated target maneuvering.

The requirement exists for a weapon system with an effective range out to about 20 km and the capability to deliver a lethal punch before the target can maneuver. A laser can provide the required results. Energy is delivered to the target at the speed of light which reduces the target's time window to maneuver. At a range of 20 km, a missile traveling at 600 m/s will move about 4 cm while the laser beam is propagating from the ship to the target. The hit is almost instantaneous which means the system need only see the target. It need not calculate an intercept trajectory prior to engagement. The energy required to kill the target and the average power of the laser will determine the dwell time, the time the laser must be focused on the target. This may range

from about 10 ms to 1 s. In either case, the target is still sufficiently far away to prevent damage to the ship. The fire control problem for maintaining the laser spot on target during the required dwell time becomes minor as the target gets closer or if the target is subsonic (nearly all sea skimmers). At a 20 km engagement range, a soft kill which merely makes the missile malfunction is as good as destroying it.

A variety of lasers exist today. They vary in wavelength, power, complexity, cost, availability and basic operation. For the most part, a laser is built for a specific purpose which dictates its wavelength and power requirements. These, in turn, affect the other variables. Once the laser is in operation, it has limited alternative uses. This is where the free electron laser (FEL) differs from the others. An FEL, once constructed, possesses the ability to operate over a wide range of wavelengths. This single fact provides a source of electromagnetic radiation at wavelengths for which no other source exists. The high average power possible from an FEL, coupled with its relatively high efficiency make it a very useful tool for science, industry and the military. In some applications all three will benefit, such as employing a ground-based laser to beam power into space for satellite usage. A specific proposal (SELENE) is discussed in Chapter II.

The free electron laser concept was first put forth by J. M. J. Madey in 1971 [1]. Relativistic electrons traveling through a periodic magnetic field can be made to give up energy to a co-propagating optical field within a resonator cavity. Figure 1.1 is a simple diagram of an FEL. The relativistic electrons are provided by an accelerator. The electron beam is then bent into the resonator cavity and directed longitudinally down the undulator by steering magnets. Magnets extract the electron beam at the other end and send it to either a beam dump or some type of energy recirculation system. The undulator is a series of magnets assembled to provide a periodic magnetic field which acts on

the electrons providing a transverse acceleration. The periodic magnetic field continuously redirects the electrons back to the center-line. Mirrors are placed at both ends of the undulator creating the optical resonator cavity. One mirror is partially transmissive to allow for the extraction of the light. If the net transfer of energy from the electrons to the optical field is positive, the optical field is amplified. The physics governing this process is discussed in Chapter III.

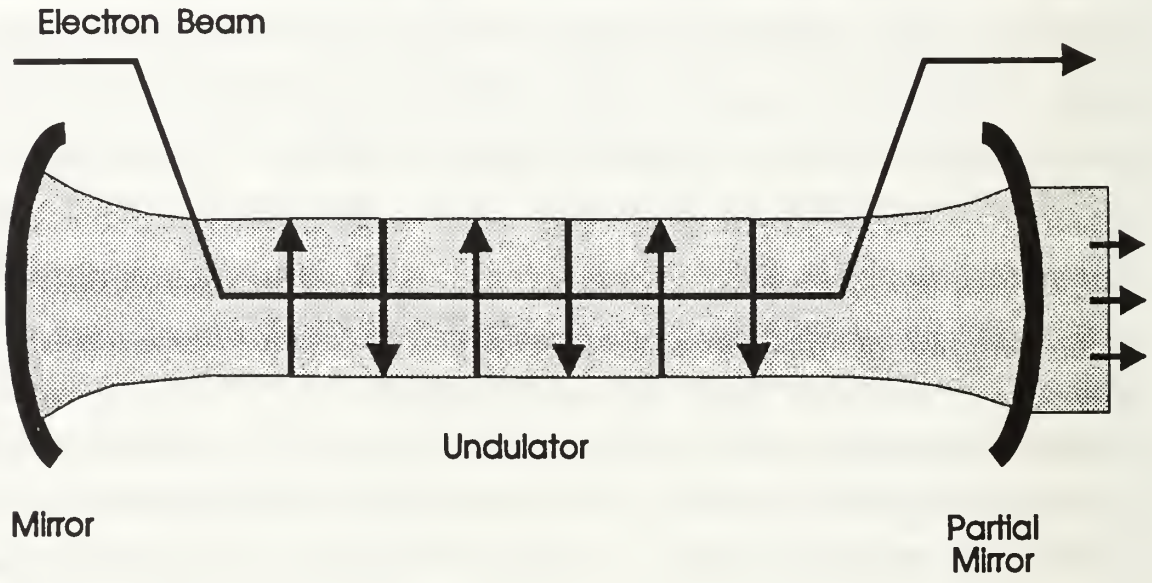

Figure 1.1 A simple FEL diagram.

Science follows a normal practice of developing new technology one step at a time. High average power laser systems are no exception. The SELENE project requires a laser with an average power never before achieved in an FEL. This leads to new designs and applications of technology. Before building the final product, a smaller scale model is necessary. The Novosibirsk proposal for a SELENE FEL is tested by the development of a slightly smaller, less complex, and less costly model which is being built for the Center for Photochemical Research in Russia. The system design and computer

simulations are addressed in Chapter IV. A free electron laser configured as an "optical klystron" is studied to determine its operating characteristics under low and high current conditions. This is addressed in Chapter V. Final conclusions for the initial design and the SELENE application are presented in Chapter VI.

II. SELENE

SELENE (**Spac**E **L**aser **ENE**rgy) is a proposal resulting from a joint National Aeronautics and Space Administration (NASA) and Department of Defense (DoD) research program to provide a means of beaming power into space [2,3]. It is appropriately named after the Greek moon goddess Selene because this technology could lead to the development of all space between the earth and the moon and of the moon itself.

A. THE SELENE PROPOSAL

SELENE utilizes a ground-based laser to convert electrical power to optical power. This optical power, in the form of a laser beam, is fed to an adaptive optics telescope which redirects the beam into space. The beam travels either directly to an end-user or to a relay mirror and then to the end-user. Figure 2.1 represents the basic system.

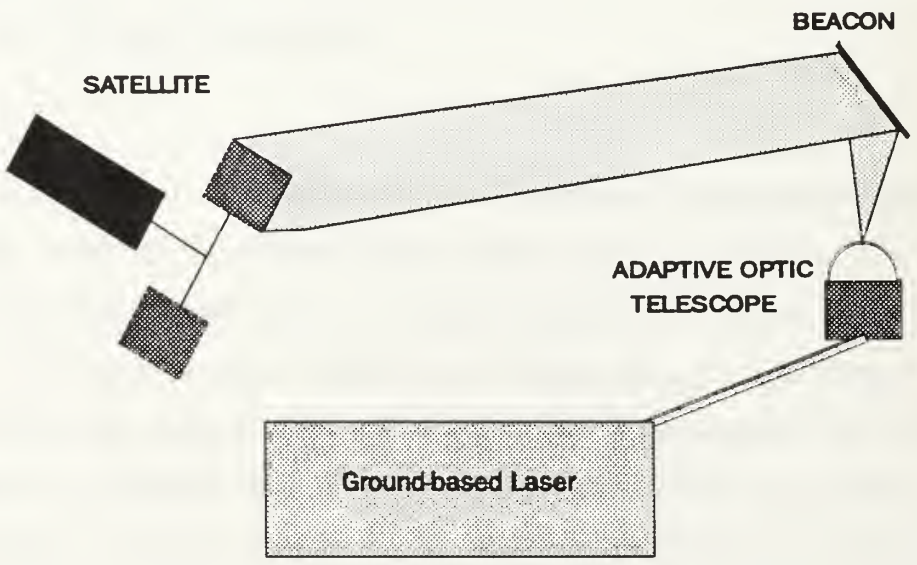

Figure 2.1 SELENE concept.

The ground-based laser must be capable of maintaining high average power over a long period of time to be useful. The free electron laser can achieve this goal. The laser uses a relativistic electron beam, a static magnetic field, and a co-propagating optical wave to generate the amplified light needed. Once the system is in operation, a steady supply of electrical power should be sufficient to keep it operating. There is no fuel storage or mixing chamber required, and no mechanical moving parts to wear out. Should the optical wavelength need to be varied for any reason, such as maximizing the efficiency of a particular type of photovoltaic cell, an adjustment of the electron beam energy may be all that is necessary.

The optical beam travels to the adaptive optics telescope via a vacuum tube approximately 2 km long. This allows the tight, high power optical beam to expand by diffraction to a beam of approximately 1 m diameter before encountering any optics. This expansion results in the power density of the beam becoming small enough to be handled by conventional optics. The optical wavefront is reshaped and the beam directed up by the adaptive optics telescope. This telescope uses a 12 m diameter segmented mirror. Each segment can be positioned individually, resulting in a surface which can shape the optical wavefront so that atmospheric distortions are nullified. The segments are positioned by a computer which samples the incoming wavefront from a guide star. The beam travels back through the atmosphere along the same path arriving with minimal distortion.

A propagation path straight up is desirable in order to minimize energy losses due to propagation through the atmosphere. The use of an aerostat with a relay mirror located at about 80 km above the telescope will allow a fairly large area of space to be covered by the beam, while significantly reducing the path length within the atmosphere, thereby reducing atmospheric losses and distortion. This reduction will simplify the adaptive optics computations.

B. SPACE-BASED USES FOR AN ENERGY TRANSFER BEAM

The requirements for electrical energy in space are currently met by employing a variety of energy collection and storage devices. Mainly, energy is collected by solar powered photovoltaic cells and stored in batteries, or provided by onboard fuel cells or nuclear power systems. Often, a combination of these provide the needed electrical power. There are, however, some drawbacks.

Batteries are heavy and make up a large percentage of the satellite payload. They are necessary though, enabling the satellite to operate during "shadow" periods when the sun's illumination is not available. Weight restraints dictate that the minimum battery storage capability necessary to ensure continuous satellite operation be provided. This results in the battery undergoing deep cyclic discharges, shortening its long-term, useful life and that of the satellite. Additionally, the photovoltaic cells are continuously bombarded with space debris, reducing their efficiency. The amount of electrical power sent to the batteries over a given time period is less. Advances in technology mean that today's satellites have a greatly expanded capability over those of ten years ago. This expanding capability necessitates an increase in the demand for electrical power. Either photovoltaic cells and storage batteries with higher efficiency and lower weights or the capability to provide additional energy to the satellite during peak usage is needed. Power beaming can meet the excess power requirements of all satellites.

Fuel cells provide the necessary fuel for station keeping, optimizing the satellite's position. As this fuel is exhausted, the satellite begins to move away from its intended position, reducing its usefulness until it is so far out of position that it is no longer useful. Now the multimillion dollar satellite is useless space junk. The time required for this to take place may be a period up to 10-12 years from satellite launch to expensive space debris. The life-time limitation

imposed on satellites by finite fuel cells need not continue. If the new satellites were fitted with electric propulsion systems, such as hydrazine electric arc jets, power beaming could provide an endless supply of power for station keeping, removing this liability to satellite life expectancy.

Currently, the cost of launching a satellite is about 6,700 dollars per pound for low earth orbit (LEO) and 72,000 dollars per pound for geosynchronous earth orbit (GEO). The economic impact of excess weight is detrimental to any satellite program. The use of a space tug with an induction ion thruster or some type of plasma thruster powered from the ground could significantly reduce the cost of putting satellites in GEO. This tug would hook up in LEO and haul the satellite out to GEO over a period of perhaps 20 days. Exact placement in orbit eliminates the need for a kicker motor which is almost as large as the satellite itself. Tremendous cost savings could be realized. Today, if a satellite is sent to GEO and malfunctions, it is lost forever. Hundreds of millions of dollars are gone with zero return. The availability of a space tug would allow the economic recovery of the satellite back into LEO where it can be repaired or retrieved by the space shuttle. The repair of the Hubble Telescope in 1993 by the crew of the space shuttle proves that the repair capability exists. Salvage of two or three expensive satellites could cover the entire cost of the SELENE power beaming system.

Looking well into the future, the development of the moon could be achieved if a cost effective power system could be provided. The SELENE system leaves all of the large, heavy parts on the earth where they can be tended to as necessary. Photovoltaic cells and batteries are all that need be transported to the moon. The continuous availability of power beamed from the earth would reduce the required battery capacity over that needed if solar illumination were the single power source. Thus an ample, reliable source of power could lead to many new technological developments in the environment

of space and the moon.

C. POWER BEAMING VERSES SOLAR ILLUMINATION

The vast majority of the power consumed by space-based systems is provided through the use of photovoltaic cells which transform the sun's electromagnetic radiation into electrical energy that is stored in batteries until needed. Figure 2.2 is a graph of this energy conversion efficiency verses radiation wavelength. The solid curves are the normalized solar spectrum. The dashed curves indicate the operating envelopes of the photovoltaic cells named with each curve. Along the top of the graph, a number of other laser sources are named with their appropriate wavelengths marked.

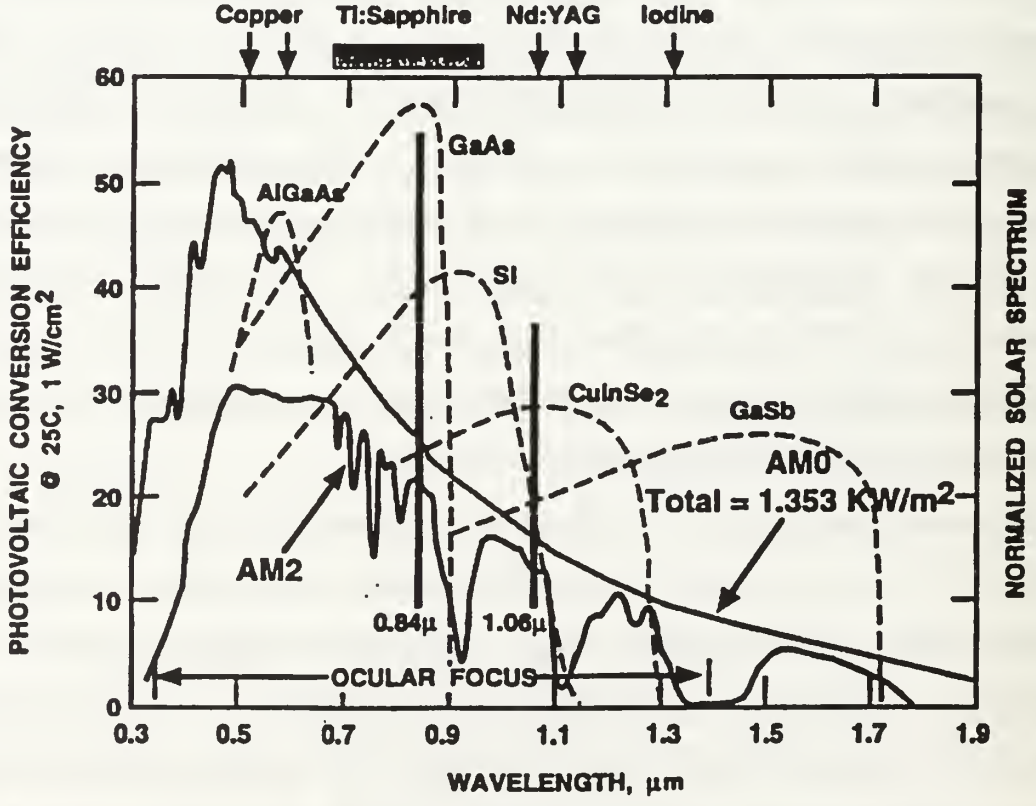

Figure 2.2 Various photovoltaic energy conversion curves for broadband solar radiation.

Common silicon (Si) cells have a broadband efficiency of 10-15%, and the newer gallium-arsenide (GaAs) cells come in at about 20-30%. Using the appropriate wavelength, Si cells will peak at 40% while the GaAs cells top out at 60%. Relatively high efficiency is achieved using a wavelength of 0.84 μm. It is evident that a power beam of proper wavelength will provide much more power over a given time frame when compared to solar illumination. This will allow the use of smaller solar panels with the satellite still receiving the same amount of energy.

Another consideration in selecting the laser wavelength is atmospheric absorption. A graph of percent transmittance verses wavelength is given in Figure 2.3. The three different plots represent different zenith angles and air masses. On a clear day and with the use of an aerostat, one can expect to achieve nearly 92% transmittance at 0.84 μm. Without the aerostat, over 80%

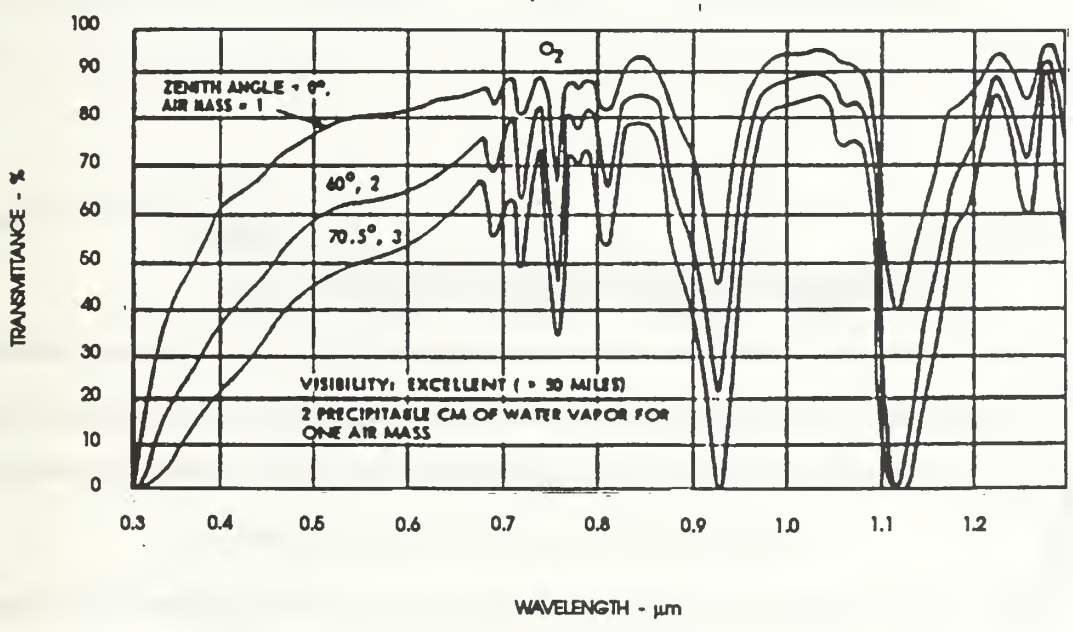

Figure 2.3 Electromagnet radiation percent transmittance through the atmosphere for various zenith angles based on wavelength.

transmittance is still possible [4]. A large portion of the high average power beam will make it into space, transferring power to the satellites.

D. NOVOSIBIRSK GROUND-BASED LASER PROPOSAL

Dr. Nikolay A. Vinokurov of Budker Institute of Nuclear Physics, Novosibirsk, Russia has made an accelerator/FEL design proposal for the SELENE project [3,5]. This design would initially provide an average power of 100-200 kW scalable to 10 MW, providing sufficient power to meet the goals of SELENE.

The Novosibirsk design proposal is illustrated in Figure 2.4. It utilizes a four pass, race-track microtron-recuperator (RTMR) feeding a relativistic electron beam into a four-section optical klystron and, finally, a single pass radiator. The electron beam would then be sent back through the RTMR to recover most of the beam energy.

The RTMR accelerator will provide an electron beam with energy on the order of 100 MeV to the optical klystron. The optical klystron is made up of four

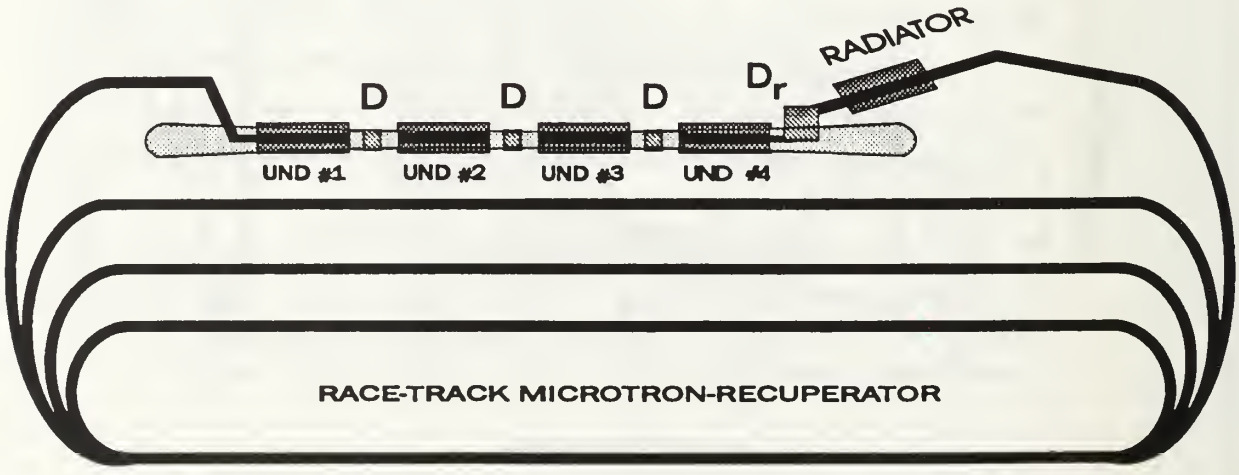

Figure 2.4 Novosibirsk FEL proposal incorporating a race-track microtron-recuperator, multi-section optical klystron and single pass radiator.

identical undulators separated by dispersive sections of equal magnetic strength. These undulators are placed between two mirrors forming the resonator cavity. Steering magnets located after the last undulator will extract the electron beam from the optical klystron and send it to a single pass radiator where the laser light used for power beaming is formed. The physics governing the optical klystron and the radiator is discussed in the next chapter.

III. FREE ELECTRON LASER THEORY

The FEL consists of three basic parts; a relativistic electron beam, a static, periodic magnetic field and a co-propagating optical field. The theory of operation can be fully discussed using classical mechanics [6]. In this discussion, a number of parameters are used which will be defined in the following section.

A. DIMENSIONLESS PARAMETERS

The static, periodic magnetic field is provided by the undulator. This is a series of magnets arranged so that the magnetic field is periodic along the longitudinal axis of the undulator. The undulator is described by the dimensionless undulator parameter $K = e\bar{B}\lambda_o / 2\pi mc^2$ where e is the electron charge, $\bar{B}$ is the undulator rms magnetic field strength, λ_o is the undulator wavelength, m is the electron mass and c is the speed of light. The distance along the longitudinal axis over which the magnetic field oscillates one full period is λ_o. The length of the undulator is $L = N\lambda_o$ where N is the number of magnetic field periods within the undulator. The electrons interact with the optical field along the entire length of the undulator. The interaction time is given by the dimensionless time $\tau = ct / L$ where $\tau = 0 \rightarrow 1$.

The relativistic electron energy is represented by the Lorentz factor $\gamma = E / mc^2$ where E is the beam energy and mc^2 is the electron rest energy. As the electron moves down the undulator, its phase with respect to the optical field is given by $\zeta = (k + k_o)z(t) - \omega t$ where $k = 2\pi/\lambda$ and $k_o = 2\pi/\lambda_o$ are the wavenumbers for the optical wavelength and the undulator wavelength, respectively, λ is the optical wavelength and $\omega = kc$. During operation, the only values that change are the electron's longitudinal position $z(t)$ and time t.

Since $k>>k_o$, the change in electron phase is $\Delta\zeta \approx k\Delta z$. The electron phase velocity is simply the dimensionless time derivative of the electron phase, $\nu(\tau) = \mathring{\zeta}(\tau) = L\,[(k+k_o)\beta_z(t)-k]$. The electron velocity in the z direction (longitudinally along the undulator) is $c\beta_z$. When $\nu = 0$, the optical and undulator field forces are resonant. The resonant optical wavelength determined by $\nu=0$ is $\lambda = \lambda_o\,(1+K^2)/2\gamma^2$.

Additional dimensionless parameters will be defined throughout this chapter as they arise.

B. ELECTRON TRAJECTORIES AND DYNAMICS

The type of undulator is determined by the magnetic field it uses. A linear undulator has a series of magnets along its length which provide a periodic magnetic field and generates linearly polarized light. The helical undulator uses coils of conducting wire wrapped around the beam line with *i* current flowing in opposite directions in alternating turns. The helical magnetic field can be represented by

$$\vec{B} = B\,[\cos(k_o z), \sin(k_o z), 0\,] \quad , \tag{3.1}$$

where B is the magnitude of the magnetic field, $k_o = 2\pi / \lambda_o$ is the wavenumber of the undulator and z is the position along the longitudinal axis of the undulator. The helical nature of the undulator allows for the cancellation of all longitudinal components of the field, leaving only the transverse components on axis.

The electric and magnetic fields of the light within the FEL are given by

$$\vec{E}_l = E\,[\cos\psi, -\sin\psi, 0\,] \quad , \tag{3.2}$$

$$\vec{B}_l = E\,[\sin\psi, \cos\psi, 0\,] \quad , \tag{3.3}$$

where E is the magnitude of the optical electric field, $\psi = kz - \omega t + \phi$ with

$k = 2\pi / \lambda$ being the optical wavenumber, λ the optical wavelength, $\omega = kc$ is the optical frequency, and ϕ the optical phase.

The forces acting on the electrons within the undulator are described by the Lorentz force equations

$$\frac{d(\gamma\vec{\beta})}{dt} = -\frac{e}{mc}(\vec{E} + \vec{\beta} \times \vec{B}) \quad , \tag{3.4}$$

$$\frac{d\gamma}{dt} = -\frac{e}{mc}(\vec{\beta} \cdot \vec{E}) \quad , \tag{3.5}$$

$$\gamma = (1 - \vec{\beta}_\perp{}^2 - \beta_z{}^2)^{-1/2} \quad , \tag{3.6}$$

where $\vec{E}$ is the optical electric field and $\vec{B}$ is the sum of the optical and the undulator magnetic fields, and $c\vec{\beta}_\perp$ is the electron's transverse velocity. The magnetic field from the undulator is the dominate field moving the electrons in the transverse direction.

Substituting (3.1), (3.2) and (3.3) into (3.4) results in

$$\frac{d(\gamma\vec{\beta}_\perp)}{dt} = -\frac{e}{mc}[E (1 - \beta_z) (\cos\psi, -\sin\psi, 0) + \beta_z B (-\sin(k_o), \cos(k_o z), 0)] \ . \tag{3.7}$$

For an FEL, $\beta_z \approx 1$ so that $E (1 - \beta_z) \ll \beta_z B$ and the transverse optical force can be ignored. The terms proportional to E are from the light only and the terms proportional to B are from the undulator only. Equation (3.7) simplifies and can be integrated to determine $\vec{\beta}_\perp$,

$$\vec{\beta}_\perp = -\frac{K}{\gamma}[\cos(k_o z), \sin(k_o z), 0] \quad , \tag{3.8}$$

assuming the electron is injected perfectly along the z-axis so the constant of integration is zero. This allows (3.5) to be solved, giving

$$\frac{d\gamma}{dt} = \frac{eKE}{\gamma mc} \cos(\zeta + \phi) \quad , \tag{3.9}$$

with $\zeta = (k + k_o) z - \omega t$ representing the electron phase. When the argument of the cosine function is positive $(-\pi/2 < \zeta + \phi < \pi/2)$, the electrons gain energy from

the optical field. When it is negative ($\pi/2 < \zeta + \phi < 3\pi/2$), the electrons give up energy to the optical field. After converting to dimensionless time, $dt = Ld\tau/c$, (3.9) becomes

$$\frac{d\gamma}{d\tau} = \frac{eKLE}{\gamma mc^2}\cos(\zeta + \phi) \quad . \tag{3.10}$$

Substituting (3.8) into (3.6) gives

$$\beta_z^2 = 1 - \frac{1+K^2}{\gamma^2} \quad , \tag{3.11}$$

which is differentiated with respect to τ resulting in

$$\beta_z \dot{\beta}_z = \frac{(1+K^2)\dot{\gamma}}{\gamma^3} \quad , \tag{3.12}$$

where $\dot{(...)} = d(...)/d\tau$. Solving (3.12) for $\dot{\gamma}$ and combining it with (3.10) yields

$$\dot{\beta}_z = \frac{(1+K^2)eKLE}{\gamma^4 mc^2 \beta_z}\cos(\zeta+\phi) \quad . \tag{3.13}$$

The electron phase differentiated twice with respect to τ gives

$$\ddot{\zeta} = L(k+k_o)\dot{\beta}_z \quad . \tag{3.14}$$

When combined with (3.13), and assuming $k \gg k_o$, the resonance condition $\lambda = \lambda_o(1+K^2)/2\gamma^2$, and recalling that $\beta_z \approx 1$, results in

$$\ddot{\zeta} = \frac{4\pi NeKLE}{\gamma^2 mc^2}\cos(\zeta+\phi) = |a|\cos(\zeta+\phi) \quad . \tag{3.15}$$

Here, $|a| = 4\pi NeKLE/\gamma^2 mc^2$ is the dimensionless optical field strength. Equation (3.15) is the electron pendulum equation which governs the electron's phase-space motion within the undulator and under the influence of the optical wave.

Recall that the electron phase velocity $v = \dot{\zeta} = L[(k+k_o)\beta_z - k] = 0$ when resonant undulator and optical field forces exist. This leads to the resonance condition $\lambda = \lambda_o(1+K^2)/2\gamma^2$. The output optical wavelength of the FEL is

controlled by K, λ_o and γ. The undulator wavelength λ_o is part of the design and is not easy to change once built. The electron beam energy γ, and undulator parameter, K, are easily altered allowing the FEL to be tuned over a large range of wavelengths.

The preceding derivation assumed perfect electron injection. This means that all electrons entering the undulator are exactly on axis and, on the average, move straight down the z-axis. This is roughly true but not exactly. The quality of the electron beam is described by the beam emittance, $\varepsilon = r_b\bar{\theta}$, where r_b is the rms initial electron radial position and $\bar{\theta}$ is the rms initial angular spread of electrons away from the z-axis. Either rms value can be altered by external focusing, but the product ε is fixed. The angular and position spreads are matched to prevent excess focusing or expanding of the beam along the z-axis by requiring $Kk_o r_b = \gamma\bar{\theta}$. This results in a maximum emittance of $\varepsilon = \gamma\lambda/2\pi NK$ [6].

Beam quality is also characterized by the spread in energy of the electrons. The initial dimensionless phase velocity of the electron, ν_o, depends on the square of the electron energy so that a spread in electron energy will result in a spread in initial electron phase velocities, $\Delta\nu = 4\pi N\Delta\gamma/\gamma$ [6].

Every electron moving into the undulator is uniquely defined in phase-space by a specific phase, ζ_o, and phase velocity, ν_o. Each electron then evolves governed by (3.15). As electrons give up energy to the optical field, their phase velocity decreases. If they take energy back out of the field, the phase velocity increases causing them to move ahead more rapidly than electrons with lower energy. This results in bunching of electrons. Equation (3.15) also indicates that the maximum energy loss by the electrons occurs in the vicinity of $(\zeta+\phi) = \pi$ resulting in an amplification of the optical wave.

C. THE SELF-CONSISTENT WAVE EQUATION

The complex optical wave equation is written as

$$\left[\nabla^2 - \frac{1}{c^2}\frac{\partial^2}{\partial t^2}\right]\vec{A} = -\frac{4\pi}{c}\vec{J}_\perp \quad , \tag{3.16}$$

where

$$\vec{A} = \frac{E(t)}{k}[\sin\psi, \cos\psi, 0] \quad , \tag{3.17}$$

and $\vec{J}_\perp$ is the transverse electron beam current and $\vec{A}$ is the vector potential for a circularly polarized plane wave. The optical phase is $\psi = kz - \omega t + \phi(t)$. Assuming the optical field amplitude and phase vary slowly, $\dot{E} \ll \omega E$ and $\dot{\phi} \ll \omega\phi$, and no x, y or z dependence, (3.17) substituted into (3.16) with all terms containing two derivatives dropped yields

$$\frac{\partial E}{\partial t} = -2\pi\vec{J}_\perp \cdot \hat{\varepsilon}_1 \quad \text{with} \quad \hat{\varepsilon}_1 = [\cos\psi, -\sin\psi, 0] \quad , \tag{3.18}$$

and

$$E\frac{\partial\phi}{\partial t} = 2\pi\vec{J}_\perp \cdot \hat{\varepsilon}_2 \quad \text{with} \quad \hat{\varepsilon}_2 = [\sin\psi, \cos\psi, 0] \quad , \tag{3.19}$$

where $\hat{\varepsilon}_1$ and $\hat{\varepsilon}_2$ are orthogonal unit vectors.

The transverse electron beam current is a summation of the contributions of individual electrons. Each electron provides

$$\vec{J}_{\perp i} = -\vec{ec}\beta_\perp \delta^{(3)}(\vec{x} - \vec{r}_i(t)) \quad , \tag{3.20}$$

with $\vec{\beta}_\perp$ from (3.8), $\vec{r}_i$ the position of the ith electron and $\delta^{(3)}(...)$ the three dimensional Dirac delta function. Taking the dot product of (3.20) with the unit vectors results in

$$\vec{J}_{\perp i} \cdot \hat{\varepsilon}_{\begin{bmatrix}1\\2\end{bmatrix}} = \frac{eKc}{\gamma}\begin{bmatrix}\cos(\zeta+\phi)\\ \sin(\zeta+\phi)\end{bmatrix}\delta^{(3)}(\vec{x} - \vec{r}_i) \quad . \tag{3.21}$$

Assuming a constant electron density ρ and summing over all sample electrons,

combining (3.18), (3.19) and (3.21) gives

$$\dot{E} = -2\pi eKc\rho < \frac{\cos(\zeta+\phi)}{\gamma} > \quad , \tag{3.22}$$

$$E\dot{\phi} = 2\pi eKc\rho < \frac{\sin(\zeta+\phi)}{\gamma} > \quad , \tag{3.23}$$

which shows that if $\dot{E} > 0$, light energy grows. This occurs at $\zeta + \phi \approx \pi$.

Recall the definition for the dimensionless optical wave amplitude, $|a| = 4\pi NeKLE/\gamma^2 mc^2$. Assuming that the electron energy stays fairly constant, the value in $|a|$ that will change with time is E. Therefore,

$$\dot{a} = \frac{4\pi NeKL^2}{\gamma^2 mc^3}\dot{E} \quad , \tag{3.24}$$

which, when coupled with (3.22) gives

$$\dot{a} = -\frac{8N(e\pi KL)^2}{\gamma^3 mc^2}\rho < e^{-i\zeta} > \quad . \tag{3.25}$$

This simplifies the wave equation to

$$\dot{a} = -j < e^{-i\zeta} > \quad , \tag{3.26}$$

where the dimensionless current density is given by $j = 8N(e\pi KL)^2\rho/(\gamma^3 mc^2)$.

For a linear undulator, the optical field goes as $a(\tau) \rightarrow a(\tau)[J_o(\xi) - J_1(\xi)]$ and the dimensionless current density goes as $j \rightarrow j[J_o(\xi) - J_1(\xi)]^2$, where $\xi = K^2/2(1+K^2)$ and J_o and J_1 are Bessel functions. An additional factor affecting the dimensionless current density is the "filling factor", $F = \pi r_b^2/\pi\omega_o^2$ which describes the cross-section overlap between the electron beam and the optical mode reducing $j \rightarrow jF$.

D. PHASE-SPACE DIAGRAMS

Electron evolution within the FEL is governed by the pendulum equation (3.15), while the optical wave evolution is governed by the wave equation (3.26). These two equations are coupled by the dimensionless current density j. The magnitude of j dictates how the optical wave will respond to the bunching of electrons within the undulator. This coupling normally holds in both weak ($|a| \ll \pi$) and strong ($|a| \geq \pi$) optical fields for high ($j \gg 1$) and low ($j \leq 1$) current.

Phase-space diagrams are useful in understanding what happens during FEL operation. The pendulum equation (3.15) is periodic within the optical wavelength, so that only one wavelength need be studied to see what is happening throughout the FEL. Phase-space is a plot of the electron's phase and phase velocity (ζ, ν) with respect to the optical wave. Figure 3.1 is such a diagram with low current $j = 1$, a moderate field $a_o = 4$ and at resonance $\nu_o = 0$.

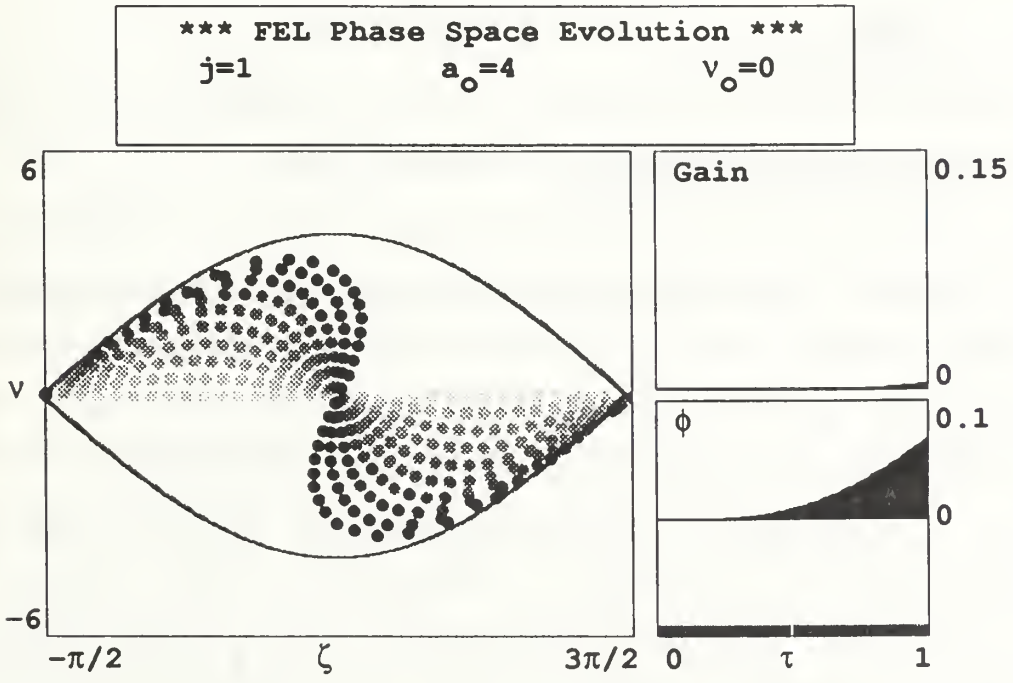

Figure 3.1 Phase-space plot for electrons entering at resonance, $\nu_o = 0$.

Each electron has an initial phase and phase velocity given by (ζ_o, v_o). These are shown in light gray. As the electrons move through the undulator, they each evolve in accordance with (3.15). On the diagram, their color darkens until it becomes black at $\tau = 1$. Since the electrons follow a simple pendulum equation, the phase-space plot can be associated with a mechanical pendulum. Unstable fixed points occur at $(3\pi/2, 0)$ and $(-\pi/2, 0)$ representing a pendulum at the top of its arc. Here, its position is farthest from center and its velocity is zero. Electrons finding themselves near these points will evolve slowly. The position $(\pi/2, 0)$ represents a stable fixed point, where the mechanical pendulum is at the bottom of its arc. The separatrix, the curved line in the plot, separates electrons with open orbits from those with closed orbits. Open orbits reflect a pendulum with sufficient energy to swing completely around and occur outside the separatrix. Closed orbits indicate periodic orbits, thus lower energy. These occur within the separatrix. The equation defining the separatrix is

$$v_s^2 = 2|a|[1 - \sin(\zeta_s + \phi)] \quad . \tag{3.27}$$

The total height of the separatrix is $4|a|^{1/2}$ relating it to the optical field strength. As light is amplified, the separatrix grows.

The two graphs on the right-hand-side of Figure 3.1 indicate the evolution of the gain and the optical phase. Gain is the fractional increase in optical power. Initially, there is no gain and no change in the optical phase. For these conditions, there is almost no gain at the end of the undulator. The phase evolution shows a change of $\Delta\phi \approx 0.1$ at the end of the undulator.

A monoenergetic electron beam will have all electrons with the same dimensionless phase velocity v_o. At resonance, $v = 0$, maximum coupling should occur. However, the electrons also have a random spread in initial phase ζ_o, so that just as many electrons gain energy as loose it. Figure 3.1

shows this balanced evolution. In order to achieve a net positive gain, the electrons should have a slightly higher phase velocity allowing them to give up more energy then they take. This is illustrated in Figure 3.2 which uses the same current and field, but a higher phase velocity $\nu_o = 2.6$. The electrons start with a phase velocity of $\nu_o = 2.6$. The electrons to the left experience an increase in phase velocity causing them to move to the right, increasing their phase position. Those to the right loose energy, reducing their phase velocity.

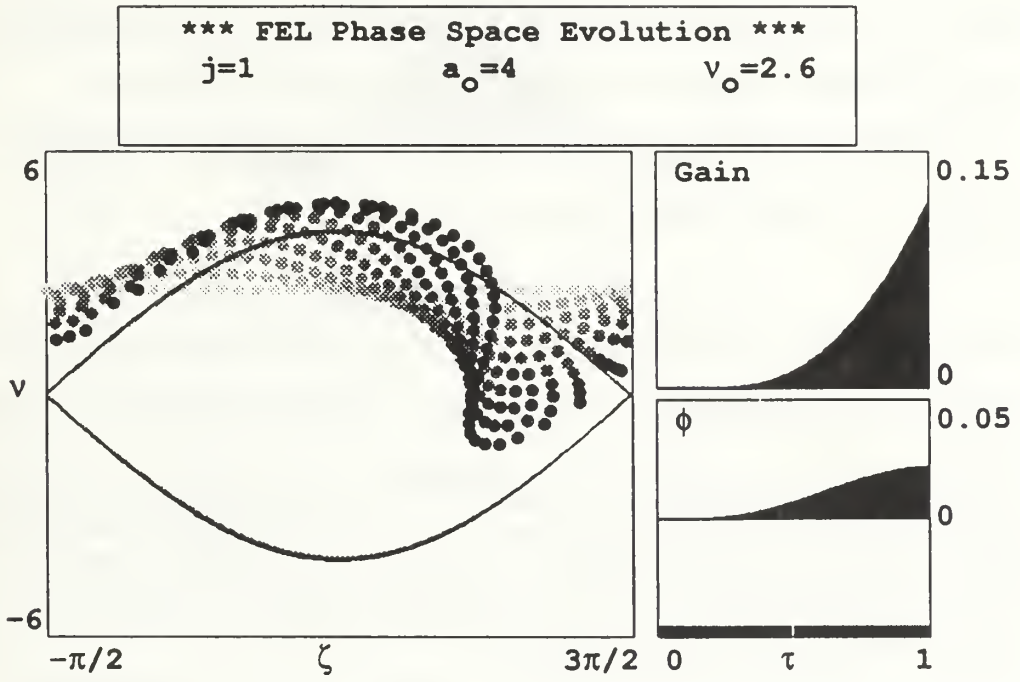

Figure 3.2 Phase-space plot for electrons entering with $\nu_o = 2.6$.

This results in spatial bunching of the electrons and coherent radiation. Now more electrons are giving up energy to the optical field than are taking energy from it. A net increase in field strength is the result. Eventually, sufficient energy will be given up with a corresponding reduction in phase and phase velocity causing the electron bunch to be in a position to start absorbing energy from the optical wave. Since the goal is to remove energy from the electrons,

amplifying the optical field, the time in the undulator should end prior to this occurring.

E. FEL GAIN

Gain represents the increase in optical field power as a function of time τ

$$G(\tau) = \frac{(a(\tau)^2 - a_o^2)}{a_o^2} \quad , \tag{3.27}$$

where a_o is the initial optical field strength at $\tau = 0$. The upper-right graph on the phase-space diagram is a graphic representation of the gain.

When the current j is low, each electron looses an average energy of $\gamma mc^2(\langle\nu\rangle - \nu_o)/4\pi N$ which results in a gain of

$$G(\tau) = j\left[\frac{2 - 2\cos(\nu_o\tau) - \nu_o\tau\sin(\nu_o\tau)}{\nu_o^3}\right] \quad , \tag{3.28}$$

assuming a monoenergetic electron beam uniformly distributed in phase. If the phase velocity is far away from resonance, $|\nu_o| \gg \pi$, the net gain will be very small. Good coupling occurs when $|\nu_o| \leq \pi$, which gives a range of about 2π. The FEL natural gain bandwidth is derived from the relation $\Delta\nu_o \approx 4\pi N\Delta\gamma/\gamma$, giving the natural gain bandwidth as

$$\left|\frac{\Delta\gamma}{\gamma}\right| \approx \frac{1}{2N} \quad . \tag{3.29}$$

Figure 3.3 is a weak-field, $a_o = 1$, low-current, $j = 1$, FEL gain spectrum and optical phase shift depiction with the phase velocity being varied from $-12 < \nu_o < 12$. The gain spectrum is asymmetric about $\nu_o = 0$ with the most gain achieved at $\nu_o = 2.6$ and the most absorption at $\nu_o = -2.6$. For each ν_o, the gain and optical phase are plotted for $\tau = 1$. The optical phase undergoes very little change when in a weak-field, low-gain regime, but the maximum change $\Delta\phi \approx 0.08$ occurs at resonance $\nu_o = 0$.

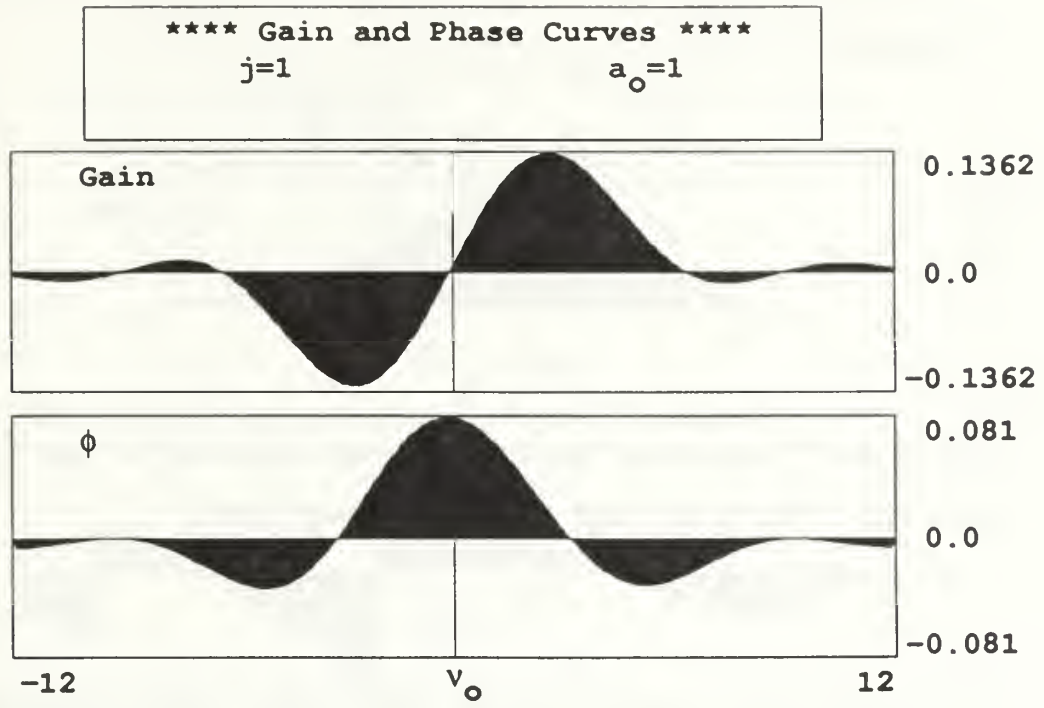

Figure 3.3 Weak-field, low-gain FEL gain spectrum and optical phase shift plot.

The gain and phase curves shift along the phase velocity axis as a function of beam energy, $\Delta\gamma \approx \gamma\Delta\nu_o / 4\pi N$ centered on the resonant energy $\gamma \approx [\lambda_o(1+K^2)/2\lambda]^{1/2}$, or optical wavelength $\Delta\lambda \approx \lambda\Delta\nu_o / 2\pi N$ centered on the resonant wavelength $\lambda \approx \lambda_o(1+K^2)/2\gamma^2$.

Higher beam current can lead to higher gain through an increase in the dimensionless current density. With an electron beam size comparable to the optical mode size, the dimensionless current density becomes $j \propto IN^3\lambda^{1/2}$. For a fixed optical wavelength, j increases with the cube of the number of undulator periods and/or as the beam current increases. This relation is not without limits, since the FEL sensitivity to energy spread and beam quality increases with an increase in N which decreases the natural gain bandwidth.

When high current density, $j \gg \pi$, is used, the complex optical field and gain equations become

$$|a(\tau)| \approx \frac{a_o}{3} e^{\left[\frac{j}{2}\right]^{1/3}\frac{\sqrt{3}\tau}{2}} , \tag{3.30}$$

and

$$G(\tau) \approx \frac{1}{9} e^{\left[\frac{j}{2}\right]^{1/3}\sqrt{3}\tau} , \tag{3.31}$$

both of which are now a function of the dimensionless current density only. Additionally, the optical phase shift becomes significant,

$$\phi(\tau) \approx \left[\frac{j}{2}\right]^{1/3}\frac{\tau}{2} . \tag{3.32}$$

As j becomes very large, the slightly higher phase velocity required for gain in the low-gain case becomes negligible and the gain spectrum centers on $\nu_o = 0$. Since gain experiences exponential growth, the gain bandwidth may be defined as the range over which the gain is reduced by $1/e$ which gives $\nu_o \approx 4j^{1/6}$.

Figure 3.4 is the gain spectrum for a moderately high-current, weak-field FEL with $j = 100$ and $a_o = 1$. The peak gain occurs at $\nu_o \approx 1.6$. As the gain has increased, the peak gain phase velocity has moved closer to resonance, $\nu_o = 0$. Additionally, the bandwidth has approximately doubled in size. The optical phase shift is also large compared to the low-gain case given in Figure 3.3.

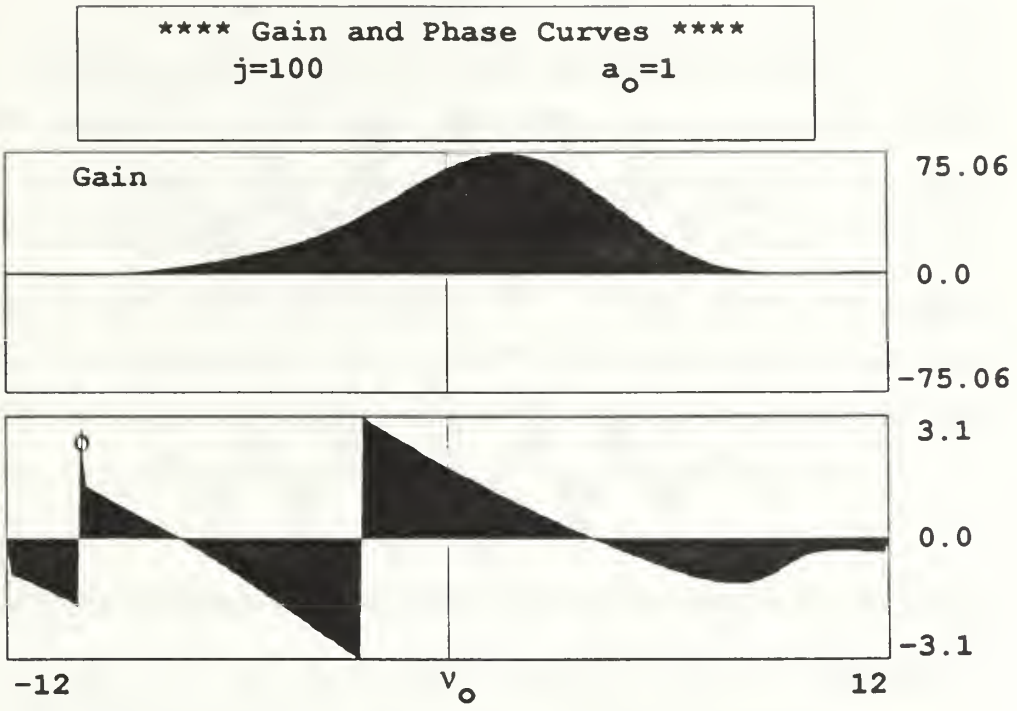

Figure 3.4 Weak-field, high-gain FEL gain spectrum and optical phase shift plot.

F. OPTICAL KLYSTRON

The purpose of configuring an FEL as an optical klystron is to increase gain in weak optical fields. In order to construct the optical klystron undulator, the undulator described in earlier sections is divided into two sections which are separated by a "drift space" or "dispersive section". The first section, called a "buncher", prepares the electrons for bunching by developing the phase velocity differences which allow the bunching to occur. The drift space is an open section which allows the electrons to continue their evolution without interaction with the optical wave. Here is where the actual bunching takes place. The second section of the undulator, the radiator, now continues the normal electron-optical wave interaction with the electrons now bunched. This is where the coherent radiation is developed.

The drift space can be achieved by two methods. The first is to have an actual distance over which the electrons travel with no light wave interaction. This is simply made, but can result in a rather large resonator cavity. The second method is to use a dispersive section, which is a magnet that forces the electrons far off centerline in an arc with a length equal to the drift distance desired. The effect is the same while the physical dimensions of the dispersive section are much smaller. The strength of either type is given by the dimensionless drift time D. This can be determined by the number of equivalent undulator periods you wish to represent through the equation

$$D = \frac{N_d}{N} \quad , \tag{3.33}$$

where N_d is the length of the drift space given in undulator periods and N is the total number of periods in the undulator.

The equations governing electron and optical wave evolution are the same as before when the electrons are within the undulator sections. This occurs during $0 \le \tau < 0.5$ and $0.5 < \tau \le 1$. At $\tau = 0.5$, the electrons are far off resonance, so the interaction does not exist. Here, the only change in electron phase is caused by the constant phase velocity, ν, of the electron as it traverses the dispersive section, $\Delta\zeta = \nu D$. The change in phase velocity of the electron is $\Delta\nu = 0$ because there is no electron-optical wave interaction. This lack of interaction allows the electrons to bunch without causing the optical field strength to grow.

Figure 3.5 is a gain spectrum and phase shift plot for an optical klystron with dispersive strength $D = 2$, weak-field, $a_o = 0.1$, and low-current, $j = 0.1$. Figure 3.6 is the same plot for a regular FEL. The differences are readily apparent. First, note that the maximum gain is approximately 6 times higher when using an optical klystron configuration. Additionally, the phase shift due to the klystron is about 4 times larger. Expressions for the gain and phase shift

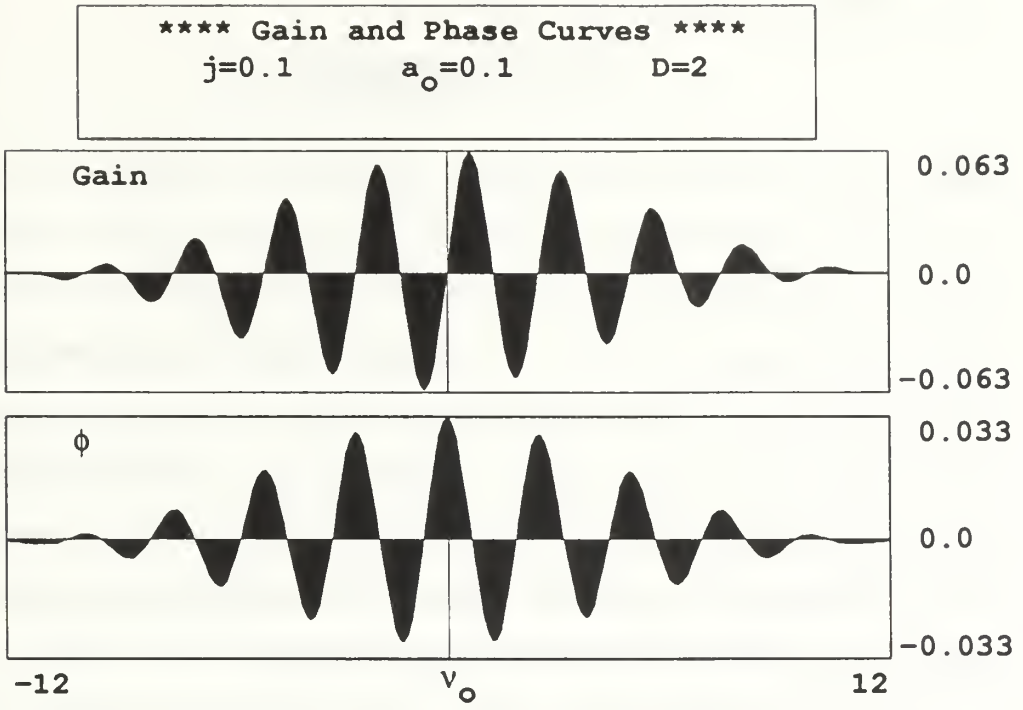

Figure 3.5 Low-current, weak-field optical klystron gain spectrum and phase shift plot.

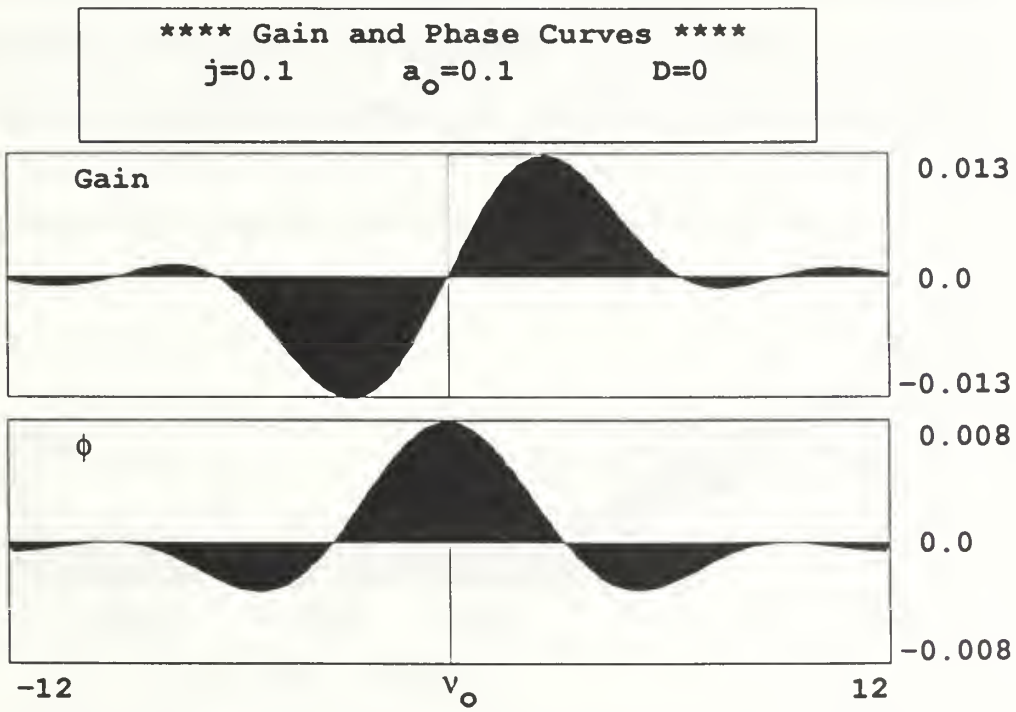

Figure 3.6 Low-current, weak-field FEL gain spectrum and phase shift plot.

when using the optical klystron are

$$G(\nu_o) \approx \frac{jD}{4} \sin(\nu_o D) \quad , \tag{3.34}$$

and

$$\phi(\nu_o) \approx \frac{jD}{8} \cos(\nu_o D) \quad . \tag{3.35}$$

The maximum gain is about $jD/4$ when $\nu_o = \pi/2D$. When the value of $D>0$, large gain can be achieved with lower values of j compared to the conventional FEL. From (3.35), the spread in initial phase velocities should be kept to $\Delta\nu_o \leq \pi/D$ which is smaller than the value required for a regular undulator. This indicates that the optical klystron is much more susceptible to electron beam quality, both emittance and energy spread.

Another feature of Figure 3.5 is the number of maximums which occur within the range $|\nu_o| \leq 2\pi$. The resulting natural gain bandwidth is another indication of the susceptibility to beam quality. The stronger the dispersive section, the tighter the requirement on beam quality. We will see that as the optical field strength increases, the benefits of the klystron are lost.

IV. NOVOSIBIRSK FEL

A team of scientists in Novosibirsk, Russia, are currently building a high average power FEL for use at the Center for Photochemical Research in Russia. This design tests the theories and technologies required to build the proposed system for the SELENE project.

A. THE PROTOTYPE

The Novosibirsk 51 MeV race-track microtron-recuperator (RTMR) [7] will provide a beam of relativistic electrons to the FEL klystron. This electron beam consists of micropulses of 20 - 100 ps in length with a repetition frequency of 2 - 45 MHz and a peak current of 20 - 100 A. The klystron and radiator are shown in Figure 4.1. The FEL klystron consists of three identical undulators of length $L = N\lambda_o$ where the undulator wavelength is $\lambda_o = 9$ cm and the number of undulator periods is $N = 40$. It is proposed that each undulator is separated from the next by dispersive magnets equivalent to $D = 0.5$. The optical resonator mirrors located at either end of the undulator are 79 m apart. The single pass radiator is an identical undulator separated from the klystron by a

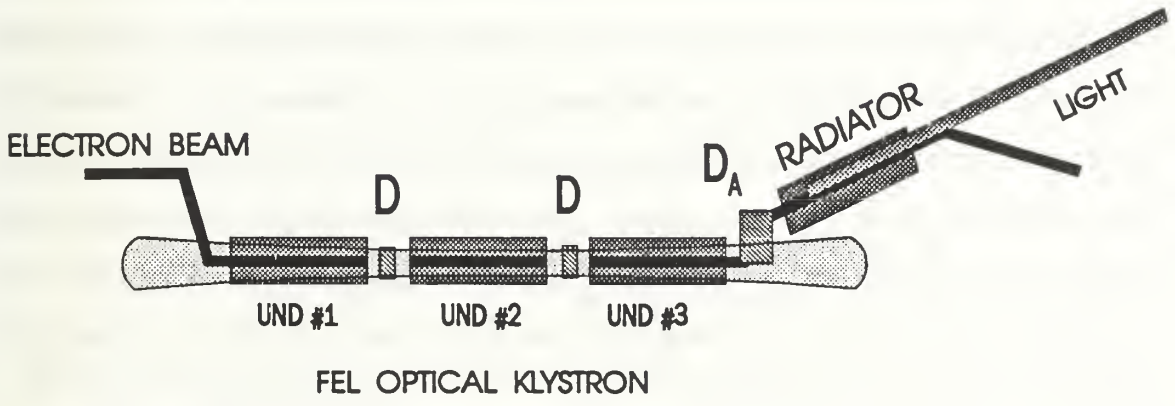

Figure 4.1 FEL optical klystron and radiator configuration.

dispersive magnet equivalent to $D = 0.25$ which imparts a 4 mrad bend on the electron beam. This bend removes the beam from the klystron oscillator and injects it into the radiator. The radiator extracts energy from the bunched electron beam beginning with spontaneous emission. The efficiency of the oscillator is limited to $\eta \approx 2\ \%$ so that the electron beam may be reintroduced into the RTMR for the recuperator phase.

The prototype has $N = 160$ undulator periods for the system (radiator and klystron), with $N = 120$ for the optical klystron alone. The undulator parameter $K = 1.4$ corresponds to an optical wavelength of $\lambda = 13\ \mu m$ with Lorentz factor $\gamma = 100$. This value of K results in $\xi = 0.3$. The total length of the undulators is $L = 1440$ cm for the system, or $L = 1080$ cm for the optical klystron. The electron beam peak current is $I = 100$ A, and the beam area is $\pi r_b^2 = 0.03\ cm^2$. The average filling factor is $\bar{F} = 0.018$ for the system and $\bar{F} = 0.023$ for the optical klystron. These values give a dimensionless current density of $j = 180$ when simulating the entire system, and $j = 100$ when simulating just the klystron oscillator.

The dimensionless klystron strength, or "drift time" D, can be varied to maximize the power out of the radiator while minimizing the power within the klystron. Initially, $D = 0.5$ for each dispersive section within the klystron and $D_r = 0.25$ for the dispersive section separating the klystron and the radiator. When simulating the klystron alone, $D = 0.67$ and $D_r = 0.33$ are used to account for the shorter total undulator length, since the dimensionless parameters are scaled to this length. The value D_r is still used with the klystron to provide an indication of the electron bunching that has taken place just prior to entering the radiator.

B. OPTICAL FIELD STRENGTH LIMITATION

The FEL klystron is designed to create electron bunching in weak optical fields. This is important because strong optical fields in the klystron oscillator would cause mirror damage. Here, we will calculate the maximum allowed optical field strength in the klystron oscillator.

A wide range of mirror materials can be used, each having its own maximum power density limit. These limits vary from 10–100 kW/cm^2. A maximum power density of $P_M = 5$ kW/cm^2 is assumed in order to assure a safety margin independent of the mirror type.

The dimensionless optical field strength at the mirrors is determined through the relation,

$$|a| = \frac{4\pi NeKLE}{\gamma^2 mc^2} = \frac{4\pi NeKL}{\gamma^2 mc^2}\left[\frac{8\pi P_M}{c}\right]^{\frac{1}{2}} \quad , \tag{4.1}$$

where $P_M = E^2 c / 8\pi$ is the optical power density. The beam spot size at the mirror w is related to the beam spot size at the waist w_o by

$$w^2 = w_o^2\left[1 + \frac{S^2}{4z_o^2}\right] \quad , \tag{4.2}$$

where the mirror separation is $S = 79$ m, and the resonator Rayleigh length is $z_o = \pi w_o^2 / \lambda$. Conservation of energy requires that $w_o^2 a_o^2 = w^2 a^2$. The maximum optical field strength within the FEL klystron is then

$$a_o = \left[1 + \frac{S^2}{4z_o^2}\right]^{\frac{1}{2}} a = \left[1 + \frac{S^2}{4z_o^2}\right]^{\frac{1}{2}} \frac{4\pi NeKL}{\gamma^2 mc^2}\left[\frac{8\pi P_M}{c}\right]^{\frac{1}{2}} \quad , \tag{4.3}$$

Using an optical beam waist of $w_o = 2r_b$ and an optical wavelength of $\lambda = 13$ μm for the prototype FEL, the Rayleigh length is $z_o = 4$ m. Equation (4.3) then

gives a maximum dimensionless optical field strength within the klystron of $a_o \approx 8$. This is well into the strong field regime, $a_o > \pi$,for both a normal FEL and an FEL klystron. In an FEL klystron, good electron bunching can be achieved at much lower values of a_o if the electron beam quality is sufficient. Therefore, if this field strength causes the klystron oscillator to saturate and operate in steady-state, it would not damage the mirrors.

C. ELECTRON BEAM QUALITY

The electron beam quality from the RTMR can be described in part by the emittance, $\varepsilon \approx r_b \bar{\theta}$ where r_b is the rms initial electron radial position and $\bar{\theta}$ is the rms initial angular spread of electrons away from the z axis. Either rms value can be altered by external focusing, but the product ε is fixed. The angular and position spreads are matched to prevent excess focusing or expanding of the beam along the z axis by requiring $Kk_o r_b \approx \gamma\bar{\theta}$. This results in a maximum emittance of $\varepsilon \approx \gamma\lambda / 2\pi NK \approx 0.2\pi$ mm-mrad for this system before the gain is reduced [8]. The design emittance of $\varepsilon \approx 0.4$ mm-mrad [9] is predicted to cause some loss in gain.

Beam quality is also characterized by the spread in energy of the electrons. The initial dimensionless phase velocity of the electron, ν_o, depends on the square of the electron energy so that a spread in electron energy will result in a spread in initial electron phase velocities. The design energy spread is $\Delta\gamma/\gamma = 0.045$ % leading to a spread in initial electron phase velocities of $\Delta\nu = 4\pi N \, \Delta\gamma/\gamma \approx 0.9$ [10].

D. SYSTEM SIMULATIONS

One-dimensional computer simulations of the FEL klystron and radiator system were conducted to determine the sensitivity of the design to the electron energy spread, $\Delta\gamma/\gamma$, and to the initial angular spread of electrons, $\bar{\theta}$, which forces a spread in initial electron position due to the fixed value of emittance.

The spread in electron energy is represented by a Gaussian distribution in phase velocity about ν_o having a standard deviation of $\sigma_G = 4\pi N\Delta\gamma/\gamma$. A Gaussian distribution in electron injection angles, assuming a matched beam, is equivalent to an exponential distribution of phase velocities with characteristic width $\sigma_\theta = 4\pi N\gamma^2\bar{\theta}^2/(1+K^2)$. Using various values of σ_G and σ_θ, simulations provide an indication of the system's sensitivity to electron beam energy spread and emittance. [6]

Figure 4.2 shows the simulation results for a single pass through the oscillator and the radiator with a mono-energetic beam and perfect beam injection ($\sigma_G = \sigma_\theta = 0$). The initial optical field amplitude, $a_o = 0.1$, is in the weak-field regime. The dimensionless phase velocity, $\nu_o = 0$, results in maximum gain for the given parameters. The dimensionless current density in the radiator is $j_r = 3500$. This value was determined by assuming a filling factor for the radiator of about $F \approx 1/3$ based on three-dimensional simulations including the effects of optical guiding [8]. The left plot shows the final position of electrons in phase-space. The upper and lower curves indicate the separatrix which delineates the regions of open and closed phase-space paths. This simulation utilizes 40 sample electrons and plots only their final positions at $\tau = 1$. The top right plot shows the optical power evolution as a function of τ along the undulator length $\tau = 0 \rightarrow 1$. The vertical axis is the natural log of the dimensionless power which is defined as $P = |a|^2$. The lower plot shows the

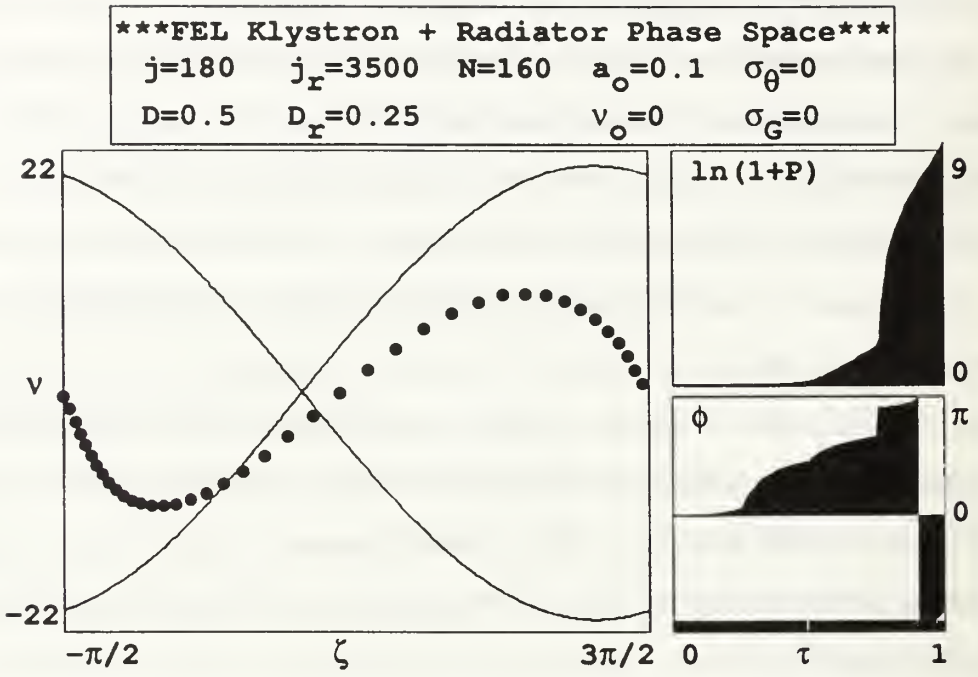

Figure 4.2 Phase-space simulation for prototype system with a perfect electron beam.

evolution of the optical phase ϕ as a function of τ along the undulator length $\tau = 0 \rightarrow 1$.

There is some increase in optical power as the electrons pass through the FEL three section klystron from $\tau = 0$ to $\tau = 0.75$. When the electrons enter the radiator at time $\tau = 0.75$, the optical field is reset to zero, but the electrons remain at their values of ζ and ν. After time $\tau = 0.75$, the power rapidly grows from spontaneous emission and amplification by the bunched electron beam, as seen in the power evolution from $\tau = 0.75 \rightarrow 1.0$. The final dimensionless power is about $P = 11{,}600$ which is equivalent to an actual peak power density of 77 MW/cm^2. The RTMR provides a continuous train of electron pulses. The pulse width divided by the pulse separation distance gives a duty factor of 0.0009. Application of the duty factor to the peak power density yields an

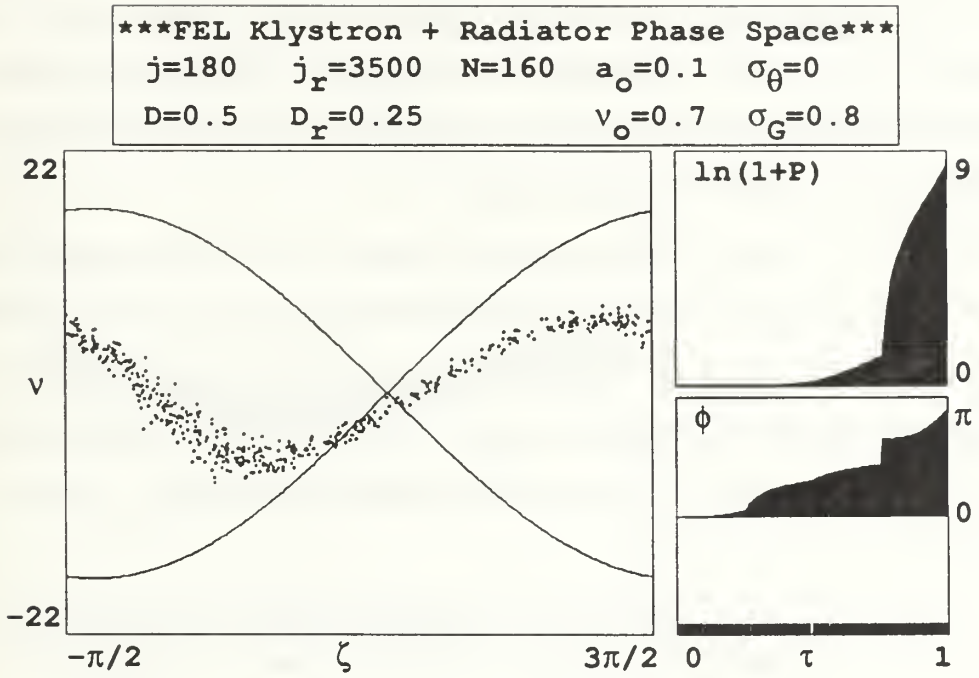

Figure 4.3 Phase-space simulation for prototype system with electron beam energy spread sufficient to reduce output by half.

average power density output of 69 kW/cm^2 for a perfect electron beam.

Values of σ_G and σ_θ that would each, independently, cause the final power out of the radiator to drop by about half were sought to provide a measure of sensitivity of the system. Figure 4.3 shows the simulation results using an electron beam energy spread $\Delta\gamma/\gamma = 0.04\%$, or $\sigma_G = 0.8$. The initial phase velocity has been adjusted to maintain maximum gain. A total of 100,000 sample electrons are used to limit the sensitivity of the simulation to shot noise. The final phase-space positions of 500 sample electrons are plotted giving a good indication of their spread. The net energy transfer from the electrons to the optical wave has been reduced. The final power has dropped to about $P \approx 5000$, which gives an average power density of 30 kW/cm^2, about half of

the value obtained with a perfect electron beam. This indicates that the prototype FEL klystron will be sensitive to electron beam energy spread. The SELENE design with an additional undulator section in the FEL klystron would require an even smaller energy spread.

Figure 4.4 shows the simulation results for a mono-energetic electron beam with a spread of injection angles given by $\sigma_\theta = 0.7$, which corresponds to an rms injection angle of $\bar{\theta} = 0.32$ mrad. The final power $P \approx 5600$ is again reduced by half from the perfect beam case. The fixed value of emittance, $\varepsilon = 0.2\pi$ mm-mrad leads to an rms initial position spread of $r_b = 2.0$ mm.

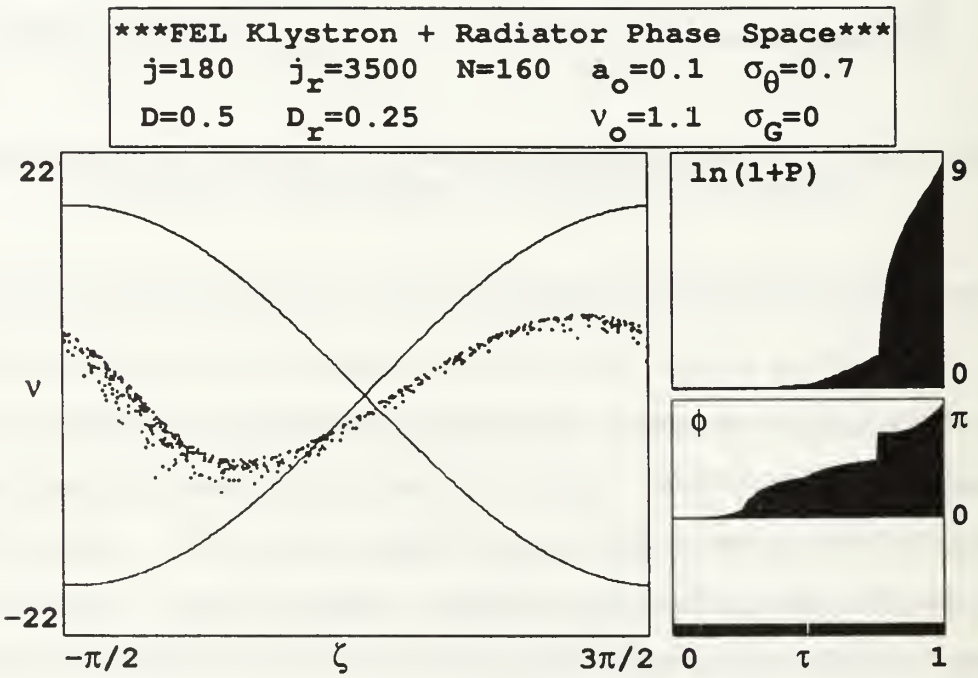

Figure 4.4 Phase-space simulation of prototype system with electron beam injection angle sufficient to reduce output by half.

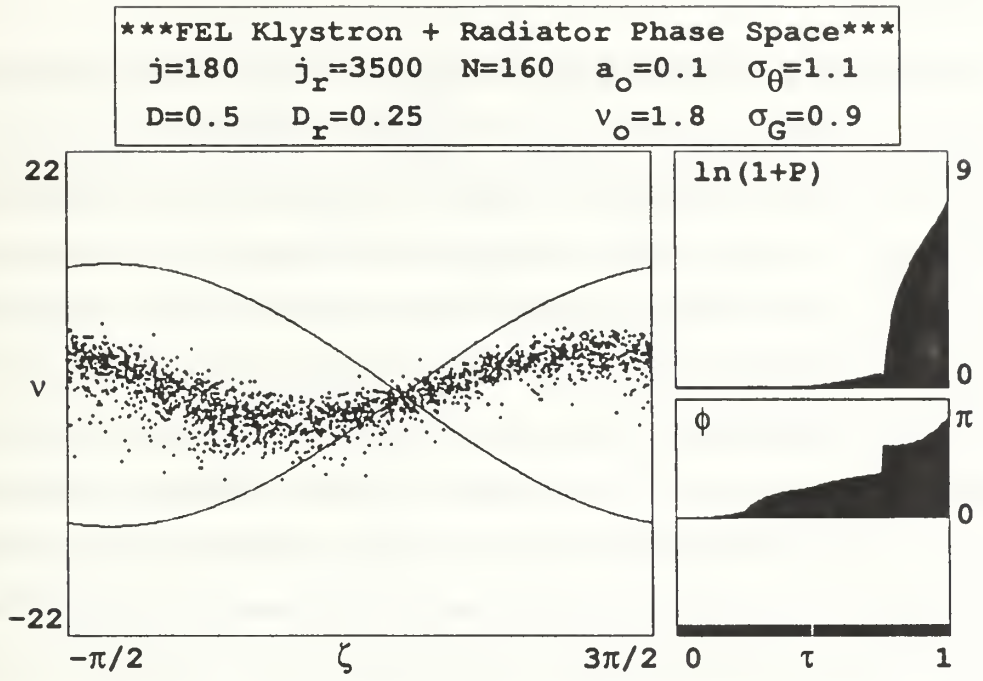

Figure 4.5 Phase-space simulation for prototype system with initial parameters for electron beam energy spread and injection angle.

The FEL klystron and radiator prototype uses estimated parameters. Figure 4.5 is a phase-space plot of the system using these values. The value of $\sigma_\theta = 1.1$ was calculated assuming an electron beam radius of $r_b = 1$ mm and the emittance fixed at $\varepsilon = 0.4$ mm-mrad. The dimensionless phase velocity ν_o has been adjusted to optimize gain as would naturally occur in the FEL klystron. The final electron positions in phase-space are spread out more than in Figures 4.3 and 4.4 due to the slightly larger values representing energy spread and emittance. The final power out is $P \approx 1280$ which gives an average power density of about 7.5 kW/cm^2. The small differences in σ_G and σ_θ cause the large difference in final power out indicating the system's sensitivity to beam quality and energy spread.

E. SUMMARY

The prototype SELENE proposal uses an FEL klystron for electron bunching. This allows the optical field strengths within the klystron to be kept low. However, the multisection klystron is sensitive to the electron beam energy spread. Adding more undulators would increase the sensitivity of the system. The power density limitations within the FEL klystron allow for strong optical fields if desired. This may allow the use of a simple undulator to provide the electron bunching reducing the sensitivity to energy spread. More simulations will be used to determine the best possible combination of parameters. Some of the parameters that can be changed are: the strengths of each dispersive magnet, the undulator lengths, the number of undulators within the FEL klystron, and the undulator field strength and the length of the radiator undulator. The large number of variables could result in more than one "best design".

V. GAIN IN THE FEL OPTICAL KLYSTRON

The FEL optical klystron referred to in Chapter IV was selected because of its ability to bunch electrons under conditions of weak optical fields, $|a| \ll \pi$. Historically, applications of the FEL optical klystron have focused on raising the gain of low current FELs driven by storage rings with $j \lesssim 1$. However, the dimensionless current density for this design is $j \approx 100$ for the optical klystron. This value is well into the high current regime. The high current FEL optical klystron may not behave like a conventional klystron and warrants further study. The research results on the high current klystron are new and are presented here for the first time. This chapter will look at the effects of high current and large D on the gain of a simple, two section optical klystron.

A. LOW GAIN

Recall the gain and phase relations given by (3.34) and (3.35),

$$G(\nu_o) \approx \frac{jD}{4} \sin(\nu_o D) \quad , \tag{5.1}$$

and

$$\phi(\nu_o) \approx \frac{jD}{8} \cos(\nu_o D) \quad , \tag{5.2}$$

which provides a peak gain of $jD/4$ at $\nu_o = \pi/D$ in the limit as $D \to \infty$ and $\nu_o \to 0$ and $jD < 1$. Figure 5.1 gives the gain spectrum and phase shift for a low-current, $j = 0.1$, weak-field, $a_o = 0.1$, optical klystron of modest strength, $D = 1$. Here, the maximum gain is 0.04 which is slightly higher than that forecast by (5.1). This fact is accounted for because D is still small. As the klystron strength is increased to larger D, the peak gain moves closer to (5.1) as is illustrated by Figure 5.2. The strength has been increased to $D = 5$, and the

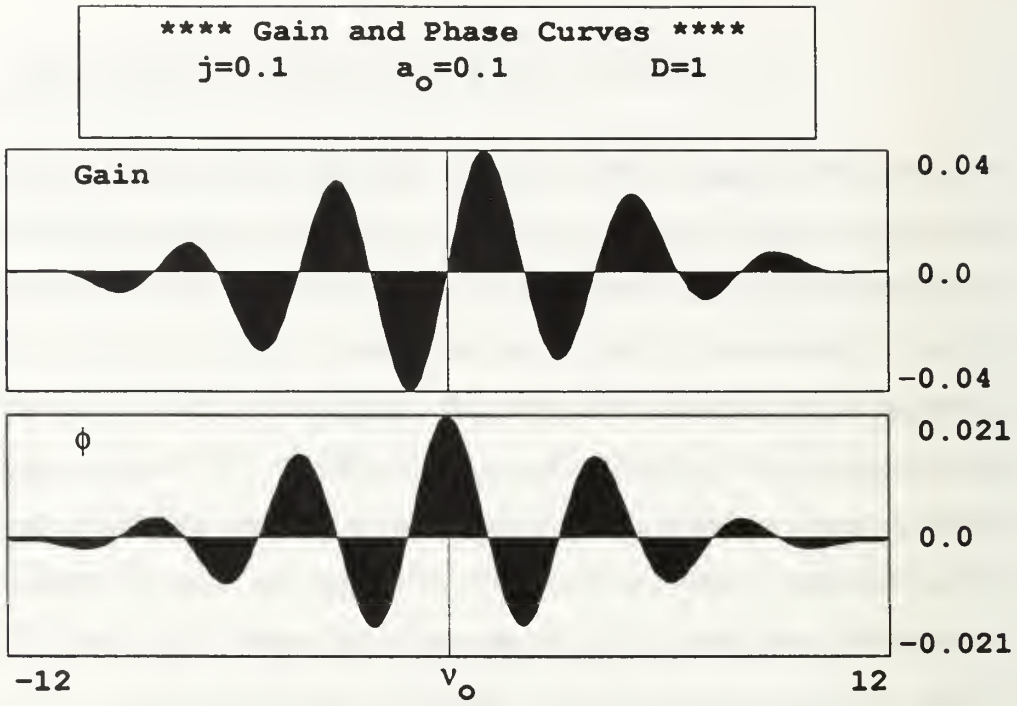

Figure 5.1 Low-current, weak-field, moderate optical klystron gain spectrum and phase shift curve.

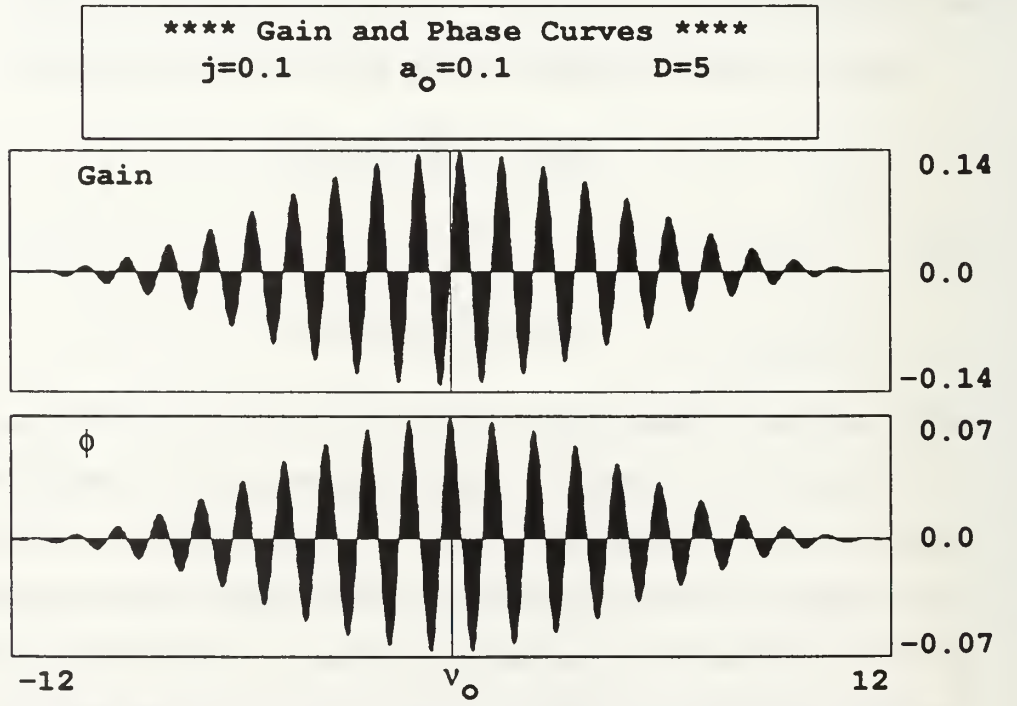

Figure 5.2 Low-current, weak-field, strong optical klystron gain spectrum and phase shift curve.

gain has increased to about 0.14, much closer to the forecast peak of 0.125. Additionally, the number of peaks within the range $|\nu_o| < 2\pi$ has increased, again indicating the sensitivity to electron beam energy spread.

Another consequence is the increase in phase shift indicated by the two figures. As the phase shift increases, it begins to affect the resonance condition which will eventually affect the gain.

B. HIGH GAIN

Increasing the product jD will increase the maximum gain and the maximum phase shift. As mentioned previously, a large phase shift will affect the resonance condition resulting in a change in the energy transfer from the electrons to the optical wave. Figure 5.3 depicts an optical klystron with a

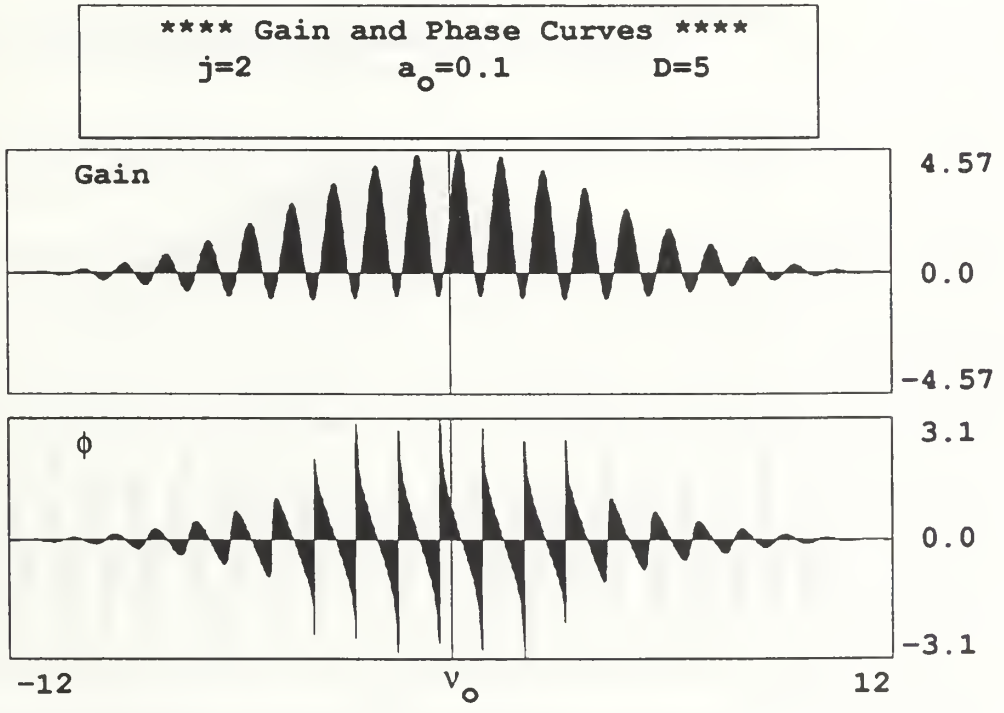

Figure 5.3 High-current, low-field, strong optical klystron gain spectrum and phase shift curve.

larger current, $j=2$, and $D=5$. The field amplitude is kept low at $a_o=0.1$. The maximum gain has increased dramatically to 4.51 which indicates the gain curve no longer follows (5.1). The phase shift has also experienced a large change, giving a maximum of 2.9. A readily apparent feature is that the gain curve is no longer asymmetric about ν_o nor does it show equal areas of radiation and absorption. At most values of ν_o, the energy flow is predominately from the electrons and into the optical field.

Increasing j even more, $j=100$, results in Figure 5.4. The optical field strength has been reduced to $a_o=0.0001$ to ensure $a_{final}<1$. The maximum gain has increased to 5476, and the areas of absorption have disappeared. The gain curve now resembles a modulated curve from a normal FEL configuration for large current, as shown by Figure 5.5, thereby losing the

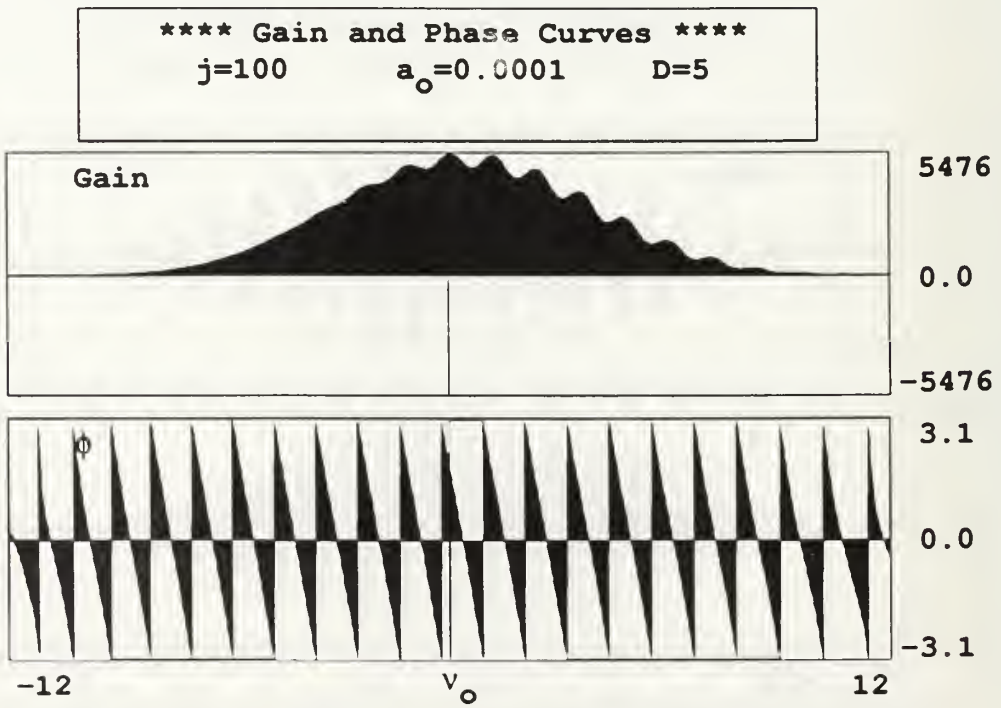

Figure 5.4 Higher-current, low-field, strong optical klystron gain spectrum and phase shift curve.

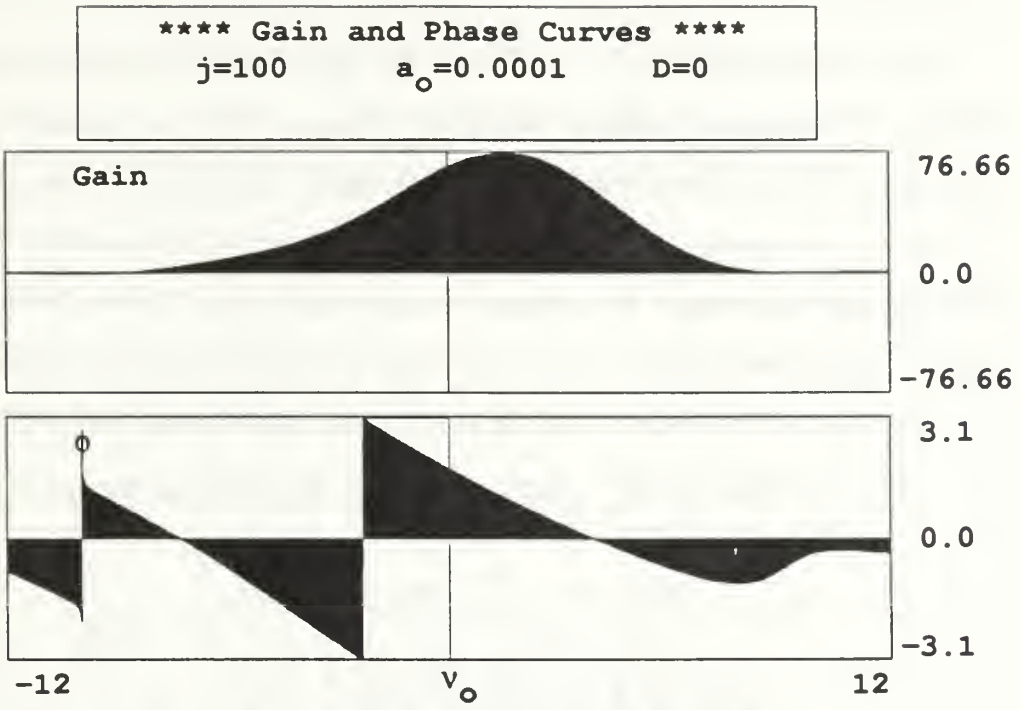

Figure 5.5 High-current, low-field FEL.

benefits of an optical klystron.

A comparison of Figures 5.4 and 5.5 indicate some interesting results. Immediately apparent is the enlarged natural gain bandwidth for the optical klystron under high current conditions. The limitations imposed on beam quality and energy spread by a low current klystron appear to be eased as the current increases. A much larger spread in ν_o will still result in net positive gain. Additionally, the maximum klystron gain, 5476, is over 70 times higher than that of a normal FEL, 76. Figure 5.4 also indicates an apparent increase in the optical field saturation level. Field saturation will be discussed in the next section.

C. SATURATION

The optical klystron will continue to amplify the field until saturation is reached. The optical field at saturation is $a_s \approx 2/D$ [11]. When $a_o \geq a_s$, the electron phase evolution becomes complicated, resulting in a decrease or loss in electron bunching and gain. Figure 5.6 shows this behavior. The optical field strength has been increased to $a_o = 5$ with $j = 0.1$ and $D = 1$. The gain curve is asymmetric with a maximum gain of 0.01 compared to 0.04 in Figure 5.1. The maximum phase shift has also been significantly reduced.

As the strength of the klystron increases, the electron distribution becomes

$$\rho(\zeta) = \rho\left[1 + \frac{a_o D}{2}\sin(\zeta - \nu_o D) + \ldots\right] \quad , \tag{5.3}$$

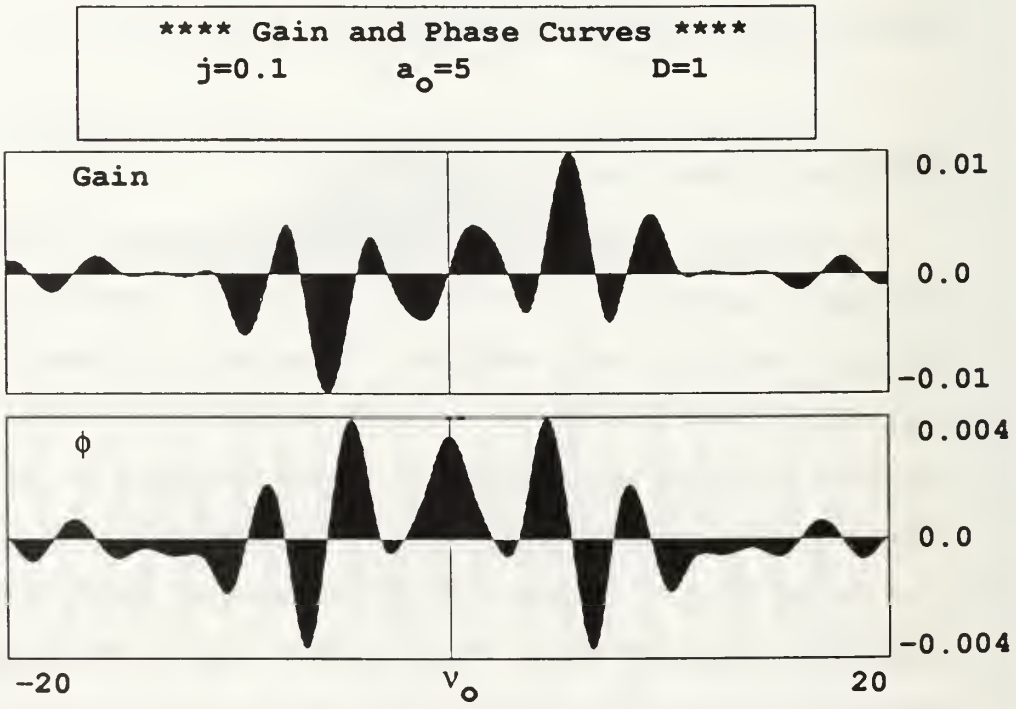

Figure 5.6 Low-current, strong-field, moderate optical klystron gain spectrum and phase shift curve.

where ρ is the electron density. As the product $a_o D$ increases, the amplitude of the modulation increases and the electrons bunch at $(\pi/2+\nu_o D) \approx \pi$ for maximum gain at $\nu_o \approx \pi/2D$. The derivation resulting in (5.1) and (5.2) only works if $a_o D \ll 1$. Therefore, the stronger the klystron, the weaker the optical fields need to be. [11]

Figure 5.7 shows an optical klystron identical to that of Figure 5.2 except that the optical field has been increased to $a_o = 1.0$. The maximum gain has dropped off to about 0.05 in stronger optical fields.

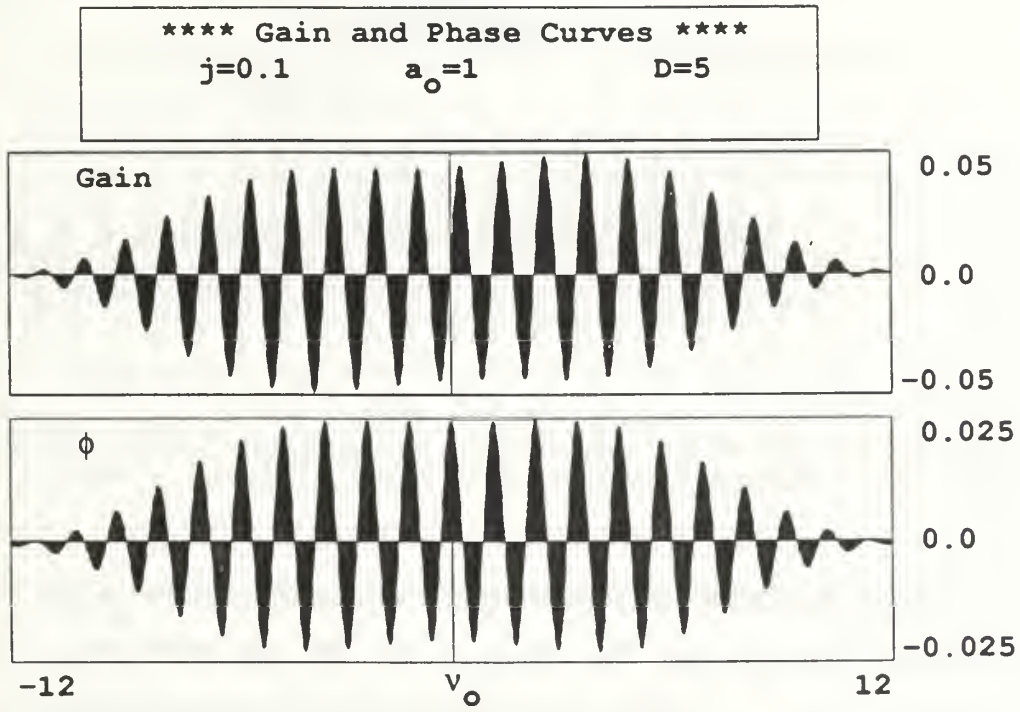

Figure 5.7 Low-current, medium-field, strong optical klystron gain spectrum and phase shift curve.

The preceding discussion dealt with low current optical klystrons. Figure 5.8 shows the results for a high current, $j = 100$, moderate field, $a_o = 1$, strong klystron of $D = 5$. When compared to Figure 5.4, the width of the spectrum has

increased, indicating a larger natural bandwidth. The curve has more structure which peaks to the right of $\nu_o = 0$. The maximum gain has decreased by about a factor of 8. The phase evolution appears to be similar.

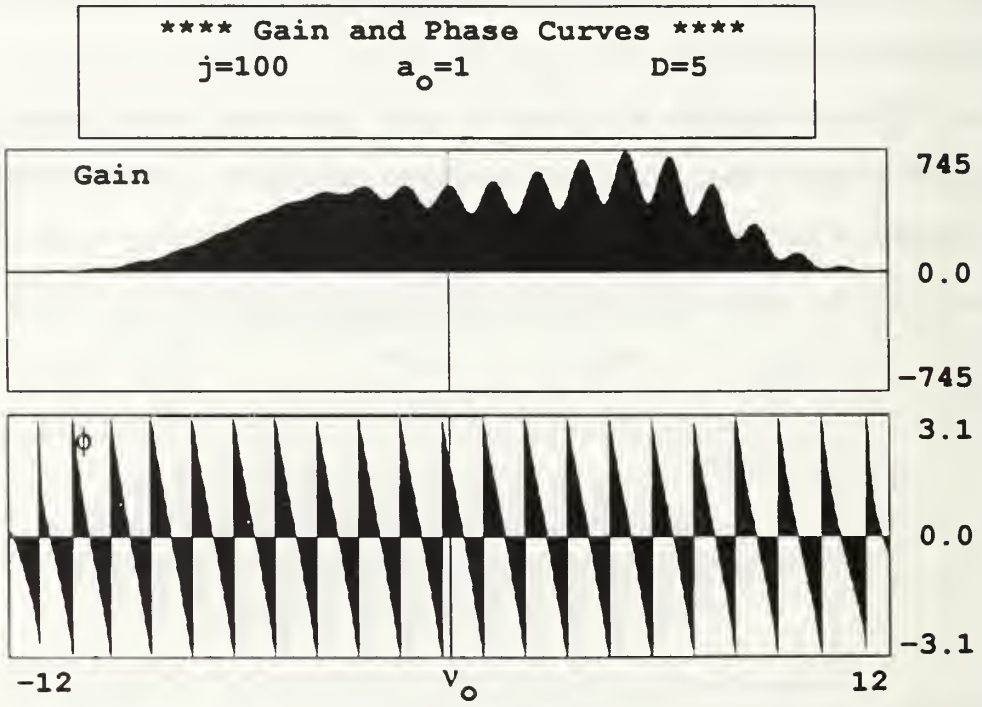

Figure 5.8 High-current, medium-field, strong optical klystron gain spectrum and phase shift curve.

Figure 5.9 is the result of the same simulation with the optical field strength increased to $a_o = 10$. The range of ν_o has been increased to show the complete curve. The width of the spectrum has increased slightly, the structure has increased markedly. The maximum gain continues to decrease; this time by almost 2 orders of magnitude. However, it is still significant gain. The phase evolution has experienced major changes. It now somewhat resembles the phase shift structure of the normal, high current FEL with superimposed rapid oscillations.

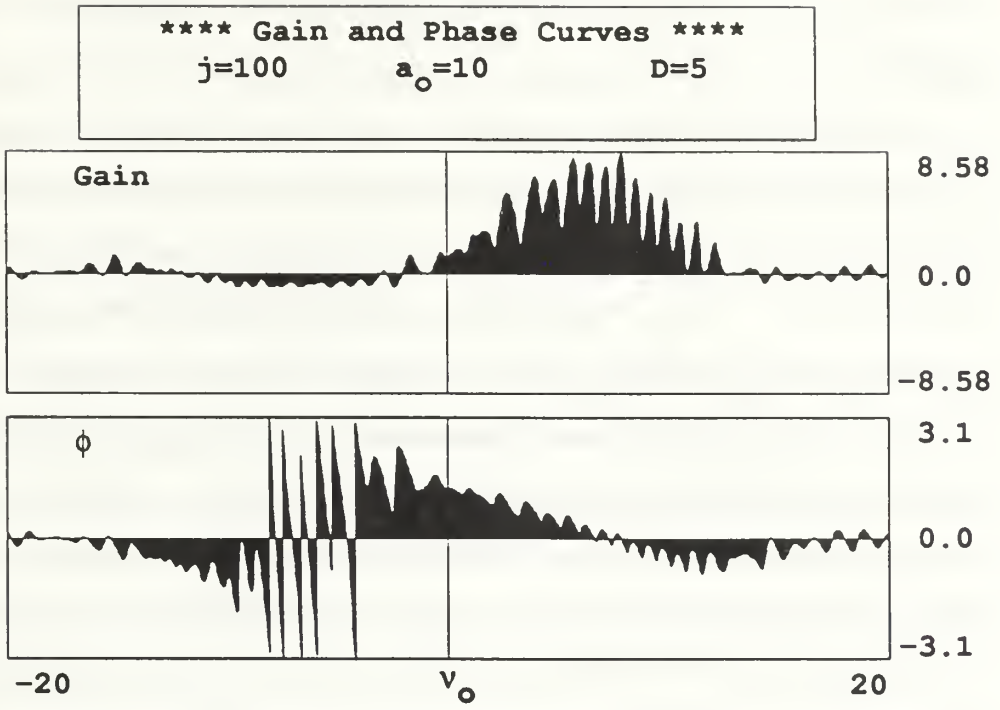

Figure 5.9 High-current, strong-field, strong optical klystron gain spectrum and phase shift curve.

When the high current optical klystron reaches saturation, the first undulator imparts a significant phase shift on the electrons. They proceed through their normal cycle of bunching and radiating while still within that first undulator. Upon reaching the second undulator, the electrons are sufficiently randomized as to effectively shut off the second undulator. This results in gain and phase curves resembling a normal, high current FEL.

D. SUMMARY

The FEL optical klystron is efficient at bunching electrons in weak optical fields. This provides the opportunity to achieve large gain in the presence of weak fields with some limitations. The maximum optical amplitude within the

resonator cavity must be kept low to prevent the degradation of the klystron benefits.

A low gain FEL klystron, limited by $jD < 1$, will achieve a maximum gain of $jD/4$ as the strength of the klystron is increased, provided a weak optical field is maintained. As the strength D is increased, the sensitivity to beam quality also increases. This may provide a limit to the maximum strength of the klystron through the users ability to provide a high quality electron beam.

If the product jD becomes greater than 1, the high gain regime is entered. Now the optical field grows significantly and the phase change is greater. This alters the resonance condition which creates an imbalance in the energy flow. More energy is transferred to the optical field with little or none being absorbed by the electrons. The field grows sufficiently to defeat the purpose for using an optical klystron, gain in the presence of weak optical fields.

In the high current optical klystron, stronger optical fields reduce the maximum gain while increasing the natural gain bandwidth. This makes them less susceptible to electron beam quality. Additionally, their gain and phase shift curves, over a range of ν_o, begin to resemble those of a high current FEL. The major difference is a much higher gain from the optical klystron.

VI. CONCLUSIONS

The proliferation of "high-tech" weapons throughout the world is fact and a matter of grave concern. These weapons may be difficult to develop but, once proven, the only requirement for possession is money. Countries of any size may acquire them for any purpose. The end result is the need for an adequate defense, capable of defeating any threat encountered.

Quantum leaps in the advancement of current weapon-systems are unexpected. Most conventional systems have been pushed to the end of their capabilities. The next step is to develop "light speed" type weapons which can engage the threat while it is sufficiently far away to preclude damage to the defending platform. The pursuit of systems capable of achieving this is slow, but advancing.

A number of laser systems exist which allow for the development of tracking and targeting subsystems. The availability of the high average power necessary for continuous engagement is still lacking. TRW has developed a chemical laser designed to fit in the volume of a 5" naval gun. This system would allow the testing and evaluating of a laser weapon system in an ocean environment. The next step appears to be a free electron laser based system.

The FEL provides the potential for high average power over a large time period. Additionally, the ability to tune it to the most affective wavelength makes the FEL a versatile weapon. Continued studies and experiments will eventually turn out system of sufficient size, weight and power to fulfill the needs of the military. Most systems today are built without concern for weight or durability. These factors must be considered in potential shipboard designs.

The SELENE project proposes to use a ground-based laser to beam power into space for a number of space-based applications and will go along way in

proving the technology. The initial goal is to achieve an average power of 200 kW, scalable to 10 MW in the future. An FEL is the most likely candidate laser for the project.

Scientists in Novosibirsk, Russia are building a laser system for use at the Center for Photochemical Research in Russia. This FEL is made up of a multisection optical klystron coupled to a single-pass radiator, fed relativistic electrons from a race-track microtron-recuperator. The system is expected to provide an average power in the kilowatt range. This will demonstrate the technology capable of meeting the needs of SELENE.

The Novosibirsk FEL optical klystron design proposes a three section klystron with a total of $N=120$ periods and a dimensionless current density of $j=100$. The strength of the klystron is $D=0.67$ for each dispersive section or 80 undulator periods worth of "drift space" each. The klystron is in the high gain regime. The gain spectrums shown in Chapter V indicate that high gain resulting from this configuration will result in strong optical fields. The purpose of this FEL klystron is to bunch the electrons while maintaining weak optical fields. The radiator will extract the necessary energy from the bunched electrons. An optical klystron with a lower current would be appropriate for this system. By reducing the number of undulator periods within the klystron by half, the current would be reduced to about $j=17$. This approach is worth further study.

The high gain and resulting large optical field within the FEL klystron will likely begin to destroy the electron bunching, thereby reducing the power extraction by the radiator. With some possible modifications, this system could prove ideal for fulfilling the needs of the SELENE project.

LIST OF REFERENCES

1. J.M.J. Madey, "Stimulated Emission Of Radiation in Periodically Deflected Electron Beams," *Journal of Applied Physics*, Vol. 42, 1971.
2. John D. G. Rather, "NASA'a Perspective on Laser Power Beaming" and E. E. Montgomery III, "System Evaluations of Laser Power Beaming Options," **Intense Laser Beams**, SPIE Proceedings Vol. 1682, R.C. Wade and P.B. Ulrich, Eds., (June 1992).
3. H. E. Bennett, John D. G. Rather, and E. E. Montgomery III, "Free-Electron Laser Power Beaming to Satellites at China Lake, California," **Laser Power Beaming**, SPIE Proceedings Vol. 2121, Jack V. Walker and Edward E. Montgomery IV, Eds., pp. 182-202, (April 1994).
4. RCA Electro-Optics Handbook, Technical series EOH-11, RCA Corporation, 1974.
5. N.A. Vinokurov, personal communication.
6. W.B. Colson, "Classical Free Electron Laser Theory", Chapter 5 in *Free Electron Laser Handbook*, W.B. Colson, C. Pellegrini and A. Renieri, Eds., North-Holland Physics, Elsevier Science Publishing Co. Inc., The Netherlands, 1990.
7. G.I. Erg, et al., "The Project of High Power Free Electron Laser Using Race-Track Microtron-Recuperator", Presented at the Fifteenth International Free Electron Laser Conference, The Hague, The Netherlands, August, 1993.

8. J. Blau, R.K. Wong, D.D. Quick and W.B. Colson, "Three dimensional Simulations of the Novosibirsk/SELENE FEL", *Nuclear Instruments and Methods in Physics Research*, North-Holland, **A341**, pp. ABS 94, 1993.

9. V.N. Litvinenko, J.M.J. Madey and N.A. Vinokurov, "Component Technologies for a Recirculating Linac Free-Electron Laser", **Laser Power Beaming**, SPIE Proceedings Vol. 2121, Jack V. Walker and Edward E. Montgomery IV, Eds., pp. 21-37, (April 1994).

10. N.A. Vinokurov, personal communication.

11. W.B. Colson and I. Boscolo, "Self-Consistent Gain in the Optical-Klystron Free-Electron Laser," *Physical Review Letters*, **A31**, No. 4, pp. 2353-2361, April 1985.

INITIAL DISTRIBUTION LIST

1.	Defense Technical Information Center Cameron Station Alexandria, Virginia 22304-6145	2
2.	Library, Code 52 Naval Postgraduate School Monterey, California 93943-5002	2
3.	Professor William B. Colson, Code PH/Cw Chairman, Department of Physics Naval Postgraduate School Monterey, California 93943-5000	6
4.	Professor Robert L. Armstead, Code PH/Ar Department of Physics Naval Postgraduate School Monterey, California 93943-5000	1
5.	Doctor Harold E. Bennett Naval Air Warfare Center Weapons Division, Code C023103 Research Department China Lake, CA 93555	2
6.	John D. G. Rather Assistant Director for Space Technology National Aeronautics and Space Administration Washington, DC 20546	1

7. Doctor Richard D. Doolittle 1
Code C321
Office of Naval Research
Ballston Center, Tower 1
800 N. Quincy St.
Arlington, VA 22217-5660